ELSEVIER

# Contents lists available at ScienceDirect

# **Biomaterials**

journal homepage: www.elsevier.com/locate/biomaterials





# Electrospun composite-coated endotracheal tubes with controlled siRNA and drug delivery to lubricate and minimize upper airway injury

Solaleh Miar<sup>a,b</sup>, Gabriela Gonzales<sup>a</sup>, Gregory Dion<sup>c</sup>, Joo L. Ong<sup>a</sup>, Ronit Malka<sup>f</sup>, Rena Bizios<sup>a</sup>, Ryan C. Branski<sup>d</sup>, Teja Guda<sup>a,e,\*</sup>

- <sup>a</sup> Department of Biomedical Engineering and Chemical Engineering, The University of Texas at San Antonio, USA
- b Department of Civil, Environmental, and Biomedical Engineering, University of Hartford, West Hartford, CT, USA
- <sup>c</sup> Department of Otolaryngology-Head and Neck Surgery, University of Cincinnati College of Medicine, Cincinnati, OH, USA
- d Departments of Rehabilitation Medicine and Otolaryngology-Head and Neck Surgery, NYU Grossman School of Medicine, New York, NY, USA
- e Department of Cell Systems and Anatomy, University of Texas Health San Antonio, San Antonio, TX, USA
- f Department of Otolaryngology Head and Neck Surgery, Brooke Army Medical Center, JBSA, Fort Sam Houston, TX, 78234, USA

#### ARTICLE INFO

#### Keywords: Endotracheal tube SMAD3 Local drug delivery siRNA delivery Upper airway

# ABSTRACT

Endotracheal Tubes (ETTs) maintain and secure a patent airway; however, prolonged intubation often results in unintended injury to the mucosal epithelium and inflammatory sequelae which complicate recovery. ETT design and materials used have yet to address intubation associated complications. In this study, a composite coating of electrospun polycaprolactone (PCL) fibers embedded in a four-arm polyethylene glycol acrylate matrix (4APEGA) is developed to transform the ETT from a mechanical device to a dual-purpose device capable of delivering multiple therapeutics while preserving coating integrity. Further, the composite coating system (PCL-4APEGA) is capable of sustained delivery of dexamethasone from the PCL phase and small interfering RNA (siRNA) containing polyplexes from the 4APEGA phase. The siRNA is released rapidly and targets smad3 for immediate reduction in pro-fibrotic transforming growth factor-beta 1 (TGF61) signaling in the upper airway mucosa as well as suppressing long-term sequelae in inflammation from prolonged intubation. A bioreactor was used to study mucosal adhesion to the composite PCL-4APEGA coated ETTs and investigate continued mucus secretory function in ex vivo epithelial samples. The addition of the 4APEGA coating and siRNA delivery to the dexamethasone delivery was then evaluated in a swine model of intubation injury and observed to restore mechanical function of the vocal folds and maintain epithelial thickness when observed over 14 days of intubation. This study demonstrated that increase in surface lubrication paired with surface stiffness reduction significantly decreased fibrotic behavior while reducing epithelial adhesion and abrasion.

### 1. Introduction

Prolonged and/or traumatic endotracheal intubation, frequently with large diameter endotracheal tubes (ETTs), substantially increases the risk of long-term voice, airway, and/or swallowing complications, with potentially life-threatening consequences such as laryngeal injury [1–6]. Laryngeal injury, defined as glottic mucosal ulceration/granulation or subglottic granulation/stenosis, was recently implicated in >50 % of patients intubated for longer than 12 h [7]. Across the world, the incidence of patients that require intubation due to respiratory failure is 13–20 million each year [8]. In addition, the rapid

spread of SARS-CoV-2 led to an unprecedented surge in the number of patients with respiratory failure who required prolonged intubation, and demonstrated that patients with severe infections are subsequently at high risk for laryngeal injury and dysfunction [9]. Subsequently, recognition of acute laryngeal injury as a functional impediment to recovery is expanding. Improved therapeutic care has reduced the risk of stenosis after prolonged intubation, with recent evidence suggesting an important role for early intervention [10]. There remains a critical need for further technological advances in therapeutic delivery to ensure such timely interventions.

Current preventive measures for posterior glottic stenosis, sub-glottic

<sup>\*</sup> Corresponding author. The University of Texas at San Antonio One UTSA Circle, AET 1.356 San Antonio, TX 78249, USA.

E-mail addresses: miar@hartford.edu (S. Miar), gabriela.gonzales@utsa.edu (G. Gonzales), diongy@ucmail.uc.edu (G. Dion), anson.ong@utsa.edu (J.L. Ong), ronit.e.malka@gmail.com (R. Malka), rena.bizios@utsa.edu (R. Bizios), ryan.branski@nyulangone.org (R.C. Branski), teja.guda@utsa.edu (T. Guda).

stenosis (SGS), or tracheal stenosis are limited to reducing duration of intubation and/or employing the smallest endotracheal tube possible. Unfortunately, both the length of intubation and endotracheal tube size are often limited by the patient's clinical condition and the potential need for adjuvant bronchoscopy or other interventions during intubation that necessitate a larger endotracheal tube. Although data suggests that early treatment for known stenosis can reduce granulation tissue and scarring [11], detailed predictive algorithms are lacking to identify patients most at risk that could benefit from prophylactic intervention. Treatment for stenosis in the upper airway include endoscopic dilations and open surgical resection [12,13]. Current treatments can often require multiple surgeries with or without tracheostomy. Adjuvant glucocorticoid use has been frequently employed, as they are known to improve airway inflammation [14-16], however current delivery approaches are mainly through intralesional and in-office steroid injection for treatment of SGS and tracheal stenosis to decrease additional fibrosis from excision of scar tissue or lesions [14,17]. Despite compelling evidence of the effectiveness of steroid injections, the application of corticosteroids to stenotic regions via in-office injections remains cumbersome and inconvenient for both patients and providers, involving flexible laryngoscopy and transcutaneous injections [14]. These treatments require repeated in-clinic procedures and subject patients to additional interventions and associated discomfort to deliver glucocorticoids over repeated doses. Furthermore, therapeutic interventions do not currently occur until after stenosis has developed, although it is well accepted that the injury is a sequela of intubation and associated damage to the airway mucosa in repeated contact with the hard surface of the ETT. Hydrogel coatings have been developed to address the stiffness of the outer surface of ETTs (such as by in situ assembly of hyaluronic acid/Pluronic F127) [18,19], which show some amelioration of mucosal damage, but Pluronic based in situ assembled hydrogels have not been conducive for facilitating simultaneous therapeutic delivery to the mucosa [20].

Stenosis of the upper airway subsequently progresses through tissue granulation to fibrosis, which results in functional deficits in voice and respiration. The application of biological modulators as therapeutic agents, specifically siRNA which targets smad3, have been studied in the preclinical setting to downregulate transforming growth factor beta 1 (TGFβ1), which has been implicated as the main pro-fibrotic signaling pathway in the development of acute laryngeal injury [21]. However, these modulators have not gained regulatory approval and controlled, targeted delivery of small molecules remains a challenge in the dynamic environment of the upper airway. Furthermore, other topically-used agents are not readily available or practical for intravenous use, due to deleterious systemic effects and need for high dosage to ensure efficacy at desired sites. Currently, there are no existing clinical technologies to directly deliver anti-inflammatory therapeutics to the laryngotracheal complex and throughout the trachea during prolonged intubation.

Treatments to facilitate prolonged delivery of therapeutics directly to the laryngotracheal tissues, preferably prior to the onset of stenosis remain unresolved. Previous studies have investigated the use of drug eluting or drug-loaded ETTs to treat airway complications locally upon intubation, focusing on delivery of analgesics [22,23], providing anti-microbial protection [24-30] and acting against inflammation and fibrosis [31-35]. Mitigation of biofilm formation, especially when associated with ventilator associated pneumonia has been the primary objective of the antibacterial coatings, as well as the embedded metallic particle surface modifications on the endotracheal tubes (extensively reviewed in Refs. [36,37]). Some of these antibacterial coatings have only been applied to the inner lumen of tubes [26,27,38,39], while others have been deposited on both the inner and outer surfaces [27,39]. Other groups have recognized that bacterial modulation can be used for its immunomodulatory effects as a preventative treatment for SGS and have implemented antimicrobial peptides as a therapeutic agent for delivery from ETT surfaces [24,32]. The other focus in improving

endotracheal tubes has been to provide temporary analgesia to reduce pain and discomfort during intubation, sometimes through simply coating analgesics (lidocaine) on the outside of ETTs [23] and in other cases through supporting sustained release [22]. However, these technologies focus on the management of bacterial infection during mechanical ventilation or pain-management over the short-term and do not target inflammatory and pro-fibrotic responses associated with mucosal injury directly. Subsequently, the controlled release of these therapeutics is not a necessity since they are intended for immediate effect or surface treatments. There have been drug eluting ETTs which employed steroids (mometasone furoate or budenoside) within electrospun fibrous coatings [31,33] or surface tethered nanoparticles [40] with sustained release to the laryngotracheal tissue to reduce airway inflammation, but increase in ETT surface roughness from coatings has been shown to increase airway inflammation. These studies emphasize the potential for two-fold functionality of efficiently coated ETTs, to prevent mechanical injury to the mucosa, and to serve as anti-inflammatory drug delivery platforms for the treatment of airway complications.

Intraluminal tracheal stent designs also hold promise for localized drug delivery; these stents, however, have limited tissue contact and limited drug-load capacity [41]. Electrospun materials have been used as drug-eluting coatings on the surface of both implanted tracheal grafts [42,43] and intraluminal stents [44,45], but these implants are intended to be resident long-term, have been shown to cause significant inflammatory sequelae without corticosteroid delivery [43,44]. These suboptimal therapeutic outcomes might be due to increased surface roughness or the stiffness of electrospun implant surfaces which are significantly stiffer than the oral mucosa they are in contact with [46,47]. Hydrogels allow for softer coatings on implant surfaces which are potentially less likely to cause an inflammatory response in the mucosa [18,28,42,48], as well as allow for rapid drug delivery of any therapeutics loaded within them. However, the use of soft hydrogel materials for drug delivery in the upper airway can pose challenges with regard to adhesion to the surface ETT and stability of the coating, leading to potential aspiration of the sloughed off material, which can pose a risk to the patient [46]. In addition, none of these technologies can effectively deliver therapeutics consistently to the complex laryngotracheal anatomy, especially at the larynx and vocal folds.

This limitation in current technology around ETTs restricts treatment capacity for ventilator-dependent patients and leaves the ETT at risk for biofilm formation and propagation of infection. Secondly, currently developed coated tubes are limited in being too stiff or too rough at the mucosal interface, causing increased inflammatory damage and prolonging recovery after extubation. We aim to transform the ETT from a functional, mechanical device to a dual-purpose device capable of delivering therapeutics to the local microenvironment, preventing longterm sequelae from prolonged intubation and providing additional therapeutic delivery in the short-term to address the underlying pathology. In this study, the proposed biphasic composite coating for ETTs consists of polycaprolactone electrospun fibers and a 4-arm polyethylene acrylate (4APEGA) hydrogel. The electrospun fibers provide a rough surface for increased attachment and retention of the softer hydrogel on the smooth ETT surface and both phases serve as drug delivery reservoirs for therapeutics with varying release kinetics. The PCL fibers allow for controlled release of dexamethasone while the soft hydrogel reduces mucosal damage and delivers the secondary antiinflammatory agent (smad3 siRNA). This biphasic system provides a platform for drug delivery with improved drug loading capacity, sustained localized release, and control over the temporal release of incorporated drugs, directly from the surface of commercially used endotracheal tubes. The novel system could potentially improve patient outcomes and reduce the risk of complications associated with intubation.

#### 2. Materials and methods

# 2.1. Drug-loaded PCL electrospun fibers fabrication and PCL-4APEGA composites preparation

To fabricate dexamethasone-loaded polycaprolactone (PCL) electrospun fibers, PCL pellets (molecular weight: 80,000) were first dissolved in chloroform and ethanol (15:85 v/v), and dexamethasone (dexamethasone:PCL w/w ratios of 2.5, 5, and 10:100) was then added to the PCL solution [49]. Final solution was then loaded into a syringe, and a syringe pump (Pump 11 Elite, Harvard Apparatus, Holliston, MA) was used to electrospin fibers (Supplementary Fig. 1). Photoinitiator 2-Hydroxy-4'-(2-hydroxyethoxy)-2-methylpropiophenone 9599) was dissolved in ethanol (0.4 % w/v) and 4APEGA (Creative PEGWorks, Chapel Hill, NC) with varying molecular weight (5k, 10k, and 20k) was dissolved in deionized water (4 % w/v). The solutions were mixed (0.1 % photoinitiator to 4APEGA v/v) and then cast on top of the electrospun fiber coated ETTs and polymerized for 5 min under ultraviolet (UV) light at 365 nm wavelength (UVP CL-1000, Ultraviolet Crosslinkers). All chemicals, unless otherwise stated, were purchased from Sigma-Aldrich (St. Louis, MO).

To load the PCL-4APEGA composites with *smad3* silencing siRNA, siRNA was first mixed with Polyethylenimine (PEI, linear, molecular weight: 20k) at a nitrogen/phosphate (n/p) ratio of 10 to mediate functional siRNA delivery while avoiding sequence non-specific effects [50–54]. Equation (1) was used to calculate the required amount of siRNA and PEI to obtain the specific n/p value [55].

$$N / P = \frac{\frac{PEI (pg)}{PEI repeat unit molecular weight}}{\frac{positive charge number}{siRNA (pg)}}$$
(Equation 1)

In a separate tube, PEI was dissolved in N-2-hydroxyethylpiperazine-N'-2-ethanesulfonic acid (HEPES) buffer of pH 7.2, followed by the addition of the siRNA amount defined in Equation (1) to the solution. The final solution was vortexed for 5 s and incubated at room temperature for 15 min to complete the complex formation. The resulting siRNA-PEI polyplex aliquot was mixed with 4APEGA polymers (molecular weights: 5k, 10k, and 20k) and photoinitiator solution followed by polymerization under UV light for 5 min as previously mentioned.

# 2.2. Morphology, swelling and stability assessment of composite coatings

Scanning Electron Microscopy (SEM) was utilized to examine the morphology of the PCL-4APEGA-coated ETTs. All specimens were lyophilized and sputter-coated with silver-palladium and imaged using an S5500 microscope (Hitachi High-Tech, Schaumburg, IL) under 20 kV applied voltage at 50x, 200x, and  $750\times$  magnifications. Samples were imaged in top view and side view of cross-section perspectives to evaluate surface morphology and layer interfaces, respectively.

Adhesion of the PCL-4APEGA coating to the ETT surface was measured using a U-Stretch tensile testing machine (CellScale Biomaterials Testing, Ontario, Canada) using methods similar to those previously reported for ETT coatings [31]. Briefly, two segments of ETT (2 cm) were placed adjacently on the rotating rod within the electrospinning setup and joined together by a fiber coating. The resulting 4 cm samples were coated with 4APEGA, clamped at the ends, and tested in displacement control mode to determine the force required to achieve slippage of the coating (n = 4 per coating). The test was performed in a temperature-controlled bath set to 37 °C and filled with phosphate buffered saline (PBS).

The frictional characteristics of the coating were evaluated using a Biomomentum Mach-1 mechanical tester v500css (Laval, Quebec, Canada) with a multi-axial load cell and 17 N amplification module. A 9 mm disc sample of ETT (n=4) was made for each PCL fiber diameter (1

 $\mu$ m, 4  $\mu$ m, and 8  $\mu$ m) and 4APEGA polymer (molecular weights: 5k, 10k, and 20k) combination. The sample was secured onto a flat indenter (MA262) with cyanoacrylate glue and put into contact with a glass microscope slide (sliding substrate) using the "Find Contact" function. A planar test over a linear path was conducted with a "Zero Load", "Stress Relaxation", and "Ramp Release" testing sequence.

The swelling rates of composites were calculated over time to compare the impact of molecular weight of 4APEGA on swelling behavior and to study the impact of swelling ratio on the drug release behavior. Dried samples (n = 6 samples per group) were weighed prior to immersion in phosphate buffered saline (PBS) buffer at 37 °C. Samples were then removed from PBS buffer at different time points and their weights were recorded after removing excess PBS. The experiment was continued until the samples reached swelling equilibrium. The swelling ratio was calculated using Equation (2), in which  $M_{\rm i}$  and  $M_{\rm f}$  are the mass of samples in its dried and swollen states, respectively.

Swelling Ratio% = 
$$\frac{M_f - M_i}{M_i} \times 100$$
 (Equation 2)

To study the degradation rate of PCL-4APEGA composites over time, samples were placed in the phosphate-buffered saline (PBS) buffer at 37 °C and observed for 14 days. Mass loss of the samples was measured weekly using Equation (3), where  $W_{in}$  and  $W_{f}$  are the initial and final sample weights of the sample, respectively.

$$\textit{Mass Loss\%} = \frac{W_{in} - Wf}{W_{in}} \times 100$$
 (Equation 3)

#### 2.3. Local mechanical characterization (microindentation)

The local stiffnesses of the composites were measured using a microindenter (Piuma Chiaro, Optics 11, Amsterdam, The Netherlands). A probe with a tip radius of  $8.5~\mu m$  and tip spring constant of 0.026~N/mwas used to measure substrate elastic modulus. Six samples per group were indented utilizing the Piuma Chiaro mapping feature in PBS at room temperature at a scan size of 9 locations (3  $\times$  3) on each sample and with a 10 µm step along both the X and Y axes. The loading and unloading force displacement curves were acquired by the instrument during each indentation process, and the Oliver Pharr model was used to calculate tip-substratum area of contact. The elastic modulus from the initial linear region of the unloading curve was then determined, assuming Hertzian contact between the indenter and substrate. Since the indentation model resulted in potentially multimodal distribution of elastic modulus across the sample substratum for composite materials, violin plots were used to tabulate the distribution of measurements and statistical testing was performed to identify differences in median values, assuming unequal variances and correcting for varying distribution profiles within populations.

# 2.4. In-vitro dexamethasone release kinetics and bioactivity

Dexamethasone released from the PCL fibers was assessed and quantified over a period of 24 days. Samples (n = 6 samples per group) were maintained in PBS buffer at 37 °C. The PBS buffer was extracted after the first 24 h and every 4 days afterwards then replaced with fresh PBS. The released dexamethasone collected in PBS was quantified by the absorbance measurement of the released dexamethasone in the PBS buffer using a plate reader (Synergy2, BioTek, Winooski, VT) at 290 nm [56]. The Kosmeyer-Peppas model was used to model the fit of the dexamethasone release within the PCL system with Equation (4), where  $M_t/M$  represent the fractional drug released at time, t, K is the release rate constant, and n is the release exponent [57]. The goodness of fit was determined by calculating the  $R^2$  coefficient to evaluate how closely the drug release followed the model.

$$\frac{M_t}{M} = K \times t^n$$
 (Equation 4)

The retention of biological activity of the released dexamethasone were determined by measuring Interleukin 6 (IL-6) and Interleukin 11 (IL-11) expression via enzyme-linked immunosorbent assays (ELISAs), as per the standard sandwich assay protocols recommended by the manufacturer. For this measurement, human tracheal fibroblasts (hTF) (Cell Biologics Inc, Chicago, IL) were pre-cultured in Dulbecco's Modified Eagle's Medium (DMEM) containing 10 % of Fetal Bovine Serum (FBS) and 1 % antibiotic-antimycotic solution (Thermofisher Scientific, Waltham, MA). Cells were maintained at 37 °C and 5 % CO2, and passaged every 3–4 days. Cells were then trypsinized after reaching  $80\,\%$ confluency and were subsequently seeded at a density of 1000 cells/well in 96-well plates. After exposure of the cells to eluted dexamethasone for 24 h, media collected from each well was used to evaluate the expression of IL-6 and IL-11. All biological reagents, unless otherwise stated, were purchased from ThermoFisher (St. Louis, MO). The proliferation rates of the hTF cells were determined after 24 h using a cell viability assay to compare the untreated control group (control), groups exposed to an aliquot of dexamethasone eluted from PCL fibers (experimental groups for bioactivity), and groups exposed to an aliquot of elution media collected from PCL fibers without any loaded dexamethasone (carrier control). The acquired microscopy images were quantified using a protocol adapted from FIJI open source image analysis software for ImageJ to calculate the number of live and dead cells [58].

# 2.5. Cell adhesion to ETT surface coating

To determine the effect of 4APEGA on cell adhesion, 3 different molecular weights of 4APEGA (5k, 10k and 20k) were mixed with photoinitiator and polymerized in 24 well plates for 5 min under sterile conditions as described previously (Section 2.1). Samples were then thoroughly rinsed with PBS and seeded with hTF cells at a density of 5000 per sample. After a 24-h incubation (at 37 °C and 5 % CO₂), non-adherent cells were removed by washing the hydrogels with PBS. To evaluate cell viability, 10 % AlamarBlue™ Cell Viability Reagent diluted in fresh growth media was added to the wells, and the plate was incubated for 4 h at 37 °C. AlamarBlue reduction was measured using a Synergy2 plate reader (BioTek, Winooski, VT), and reported by normalizing to the bare ETT. Samples were then imaged using Leica DM8000 M (Buffalo Grove, IL) after fixing with 4 % paraformaldehyde for 1 h and stained using the ActinGreen™ 488 ReadyProbes™ and diamidino-2-phenylindole (DAPI).

# 2.6. Simulation of mucosal damage during intubation

To study the abrasion of the inner lining of trachea during intubation, fresh porcine tracheae were harvested (from animals euthanized in an unrelated preclinical study) to develop an ex-vivo model. To measure the impact of 4APEGA friction on epithelial abrasion of the inner lining of tracheae over 7 days, the trachea's inner lining (distant from the bronchial branch point) was separated from the tracheal cartilage rings, sectioned into 16 pieces, and split into four main experimental groups. To mimic the friction between the coated-ETTs and the epithelial mucosa, a mechano-culture MCT6 loading system (CellScale; Ontario, Canada) was programmed to apply cyclic strain of 10 % at a frequency of 0.2 Hz in a sinusoidal waveform to simulate physiological breathing in the human lung (Supplementary Fig. 2). Tissue segments were then loaded into a custom-built chamber containing 50 % (volume) hTF growth media mixed with 50 % (volume) Airway Epithelial Cell Basal Medium containing the supplementary Bronchial Epithelial Cell Growth Kit. The composites and bare ETTs (negative control) were connected to the MCT6 loading system. The hydrogels were kept in contact with tissue segments and the loading system applied cyclic strain for up to 7 days. After loading, part of tissue samples was obtained using a biopsy punch (diameter: 0.15 cm) and homogenized in 500  $\mu l$  of PBS. To lysate the tissue, 500 µl of radioimmunoprecipitation assay buffer (RIPA 1X) containing protease inhibitors was added to the homogenized tissue and

agitated at room temperature for 30 min, followed by centrifuging at 1000 rpm for 5 min to remove tissue debris. Lubricating mucin glycoproteins (MUC5b and MUC5AC) of the upper airway were then quantified via ELISA using the manufacturer's recommended protocol (Novus Biologicals, Centennial, CO). The remaining tissue segments were fixed in 4 % paraformaldehyde solution for histological evaluation. After the samples were fixed, they were perfused with 15 % sucrose solution at 4 °C for 6 h followed by an overnight perfusion in 30 % sucrose solution at 4 °C to reduce possible damage during the cryosectioning step. Then, samples were mounted in disposable embedding molds filled with optimal cutting temperature compound Scigen Tissue-Plus (Fisher Scientific, Hampton, NH) and the molds were stored at -80 °C prior to sectioning. Frozen tissue segments were cut to a tissue thickness of 8  $\mu m$ using a cryostat (CM1850, Leica, Wetzlar, Germany) and thaw-mounted on glass slides. Slides were maintained at room temperature overnight to dry. To improve the adhesion of the tissue slices to the glass slides, slides were kept in chilled acetone at  $-20^{\circ}$ C for 10 min. Subsequently, slides were hydrated with deionized water prior to staining. To observe possible epithelial abrasion, tissue segments were stained with Alcian Blue and Fast Red Nucleus to visualize the mucus layer. Samples were first stained with Alcian Blue 8G solution (1 % (w/v) Alcian Blue in 3 % (v/v) acetic acid/deionized H<sub>2</sub>O (pH 2.5)) for 15 min and washed three times to remove excess stain from the slides. The slides were then counterstained with Fast Red Nucleus for 5 min and washed with deionized water three times for 1 min before mounting with ProLong Diamond Antifade Mountant. Finally, the stained tissue sections were imaged with the Lionheart microscope (BioTek, Winooski, VT) at 4X and 10× magnification.

# 2.7. SiRNA-PEI polyplex release, transfection and gene-silencing efficacy

4APEGA hydrogels with varying molecular weights (5k, 10k, and 20k) combined with siRNA-PEI polyplex were incubated in PBS at 37 °C. The release of siRNA was monitored at different time intervals over a 24 h period. PBS buffer was removed at each time point and replaced with fresh PBS. Each sample containing the siRNA polyplex was centrifuged for 15 min at maximum speed and the siRNA content was measured using Quant-iT<sup>TM</sup> RiboGreen® assay as per the manufacturer's recommended protocol.

The transfection efficacy and gene silencing potential of released siRNA-PEI polyplex on hTF cells was compared with hTF cells exposed to a non-sense siRNA group (negative control), free siRNA targeting smad3, and the free polyplex before loading into the hydrogels. For this experiment, hTF cells were initially cultured in DMEM containing 10 % of FBS and 1 % antibiotics (penicillin-streptomycin - amphotericin cocktail), incubated at 37 °C and 5 % CO<sub>2</sub>, and passaged every 3–4 days. T-150 mm flasks were seeded with  $1 \times 10^6$  cells and maintained at 37 °C and 5 % CO2 to reach 80 % confluency before being treated with 100 pmol of siRNA followed by TGFβ1 exposure [59]. The cells were subsequently lysed using TRIzol™ Reagent and total RNA was extracted using RNeasy Mini Kit (Qiagen, Valencia, CA). RNA concentration and quality was evaluated using a Take 3 Micro-Volume Plate (Biotek, Winooski, VT) and spectrophotometer. Next, RNA was reverse transcribed with iScript<sup>TM</sup> cDNA Synthesis Kit (Bio-Rad, Hercules, CA). Using a fixed amount of complementary DNA (cDNA) with iTaq Universal SYBR Green Supermix (Bio-Rad, Hercules, CA), real-time reverse transcription polymerase chain reaction (RT-PCR) was performed using a CFX96 Touch Real-Time PCR Detection System (Bio-Rad, Hercules, CA). The data was analyzed using the  $2^{-\Delta\Delta Ct}$  method in which the non-sense group was designated as the baseline group and gapdh expression was used as the loading control. Predesigned smad3 primers (Sigma-Aldrich) were used to study the transfection efficacy of the polyplex with different n/p values. Table 1 shows the specific forward and reverse primers sequences for the tested *smad3*.

**Table 1**PCR primer sequences.

Target Gene	Sequence (5'-3')
SMAD3	F- CATCGAGCCCCAGAGCAATA
SMAD3	R- GTGGTTCATCTGGTGGTCACT

# 2.8. Dual drug release impact on fibrosis

Released polyplex and dexamethasone from endotracheal tubes coated with 4APEGA-PCL were tested on hTF cells to study the impact of dual drug release on fibrosis gene expression. hTF cells were treated with drugs aliquot for 24 h, followed by treating the cells with fresh media containing TGF $\beta$ 1 (10 ng/ml) for 24 h for cell stimulation. Lysis was then performed using TRIzol<sup>TM</sup> Reagent and the expression of 84 genes (Supplementary Table 1) related to encoding inflammatory cytokines, ECM remodeling enzymes, TGF $\beta$  signaling molecules were quantified using the Human Fibrosis RT2 Profiler PCR Array (Qiagen) and the clustergram heat map for relative magnitude of gene expression were generated using the Complex Heatmap package in R (version 4.1.3) [60,61].

# 2.9. In-vivo study

The Bridge Preclinical Testing Services Institutional Animal Care and Use Committee (protocol BPTS-21-01) approved the current study. Traumatic intubation was simulated in 9 Yorkshire crossbreed swine under direct laryngoscopy and 5 cm segments of composite coated ETTs (4 µm PCL fiber- 4APEGA, MW 20k) were secured in the airway for localized delivery of therapeutics for 3, 7, or 14 days (n = 3 per timepoint). The control groups of ETTs coated with 4  $\mu m$  PCL fiber only and loaded with dexamethasone, or bare ETTs without drugs have been previously reported in part [62]. Swine were anesthetized via intramuscular Telazol® and Ketamine 2.2 mg/kg and maintained using 0.5-5% isoflurane throughout the procedure. Buprenorphine 0.01-0.05 mg/kg was used for analgesia. A round 3/8 in. stainless steel brush was used for mucosal injury to the laryngeal tissue under endoscopic visualization. A second surgeon assisted with ETT placement. Briefly, two 16G angiocatheter needles were placed into the airway through the cricothyroid membrane and between the first and second tracheal rings. A snare (Amplatz Gooseneck Microsnare Kit, Medtronic PLC, Minneapolis, MN) was then passed through the angiocaths to the surgeon performing direct laryngoscopy who then secured the 5 cm ETT segment using a 2-0 polypropylene suture. The ETT was then pulled into the larynx by retracting the snare and sutures through the angiocaths. Once visually assessing the correct placement of ETT, the sutures were secured to the neck over a surgical button and incisions were closed using 4-0 polygalactin suture and Dermabond. Following ETT placement animals were monitored post-operatively hourly for the first 4 h after surgery, every 4 h for the first 24 h, and then twice daily until end of study timepoints. Animals were euthanized with pentobarbital infusion (100 mg/kg) and confirmed via vital sign monitoring according to institutional protocol. The larynx was excised immediately after euthanasia, sectioned in the sagittal plane, and frozen at  $-80\ ^{\circ}\text{C}$  until further investigation.

# 2.10. Mechanical characterization of injured laryngeal tissue

Local stiffness outcomes were determined with normal indentation using a Biomomentum Mach-1 v500css with a single-axis load cell (1.5 N) with amplification module as previously described by our group [63, 64]. Bisected larynges were fixed into a Plaster of Paris mold, aligned to a template with pre-determined indentation points along the vocal fold and submerged in PBS. Normal indentation was conducted using a 2 mm spherical indenter tip with a set velocity of 1.2 mm/s and an indentation depth of 0.3 mm. Tissue stiffness was determined from the resulting

force vs. displacement curves.

# 2.11. Histological analysis

Following mechanical analysis, 5 mm sections were taken along the mid-region of the vocal fold and fixed in 4 % formalin overnight. Tissue samples were mounted in disposable embedding molds using optimal cutting temperature compound (Thermo Fisher Scientific, Waltham, MA), sectioned to a thickness of 14 µm using a cryostat (Epredia™ NX70, Kalamazoo, MI), and stored in −80 °C until staining. Slides were stained with hematoxylin and eosin (H&E) (Richard-Allan Scientific™ Signature Series™ Stains, Thermo Fisher Scientific, Waltham, MA) according to the manufacturer's protocol. Slides were imaged at 20X using a Motic EasyScan Pro Slide Scanner (Motic Instruments, Schertz, TX). Epithelial thickness along the vocal fold was measured in ImageJ (Version 1.53k, National Institute of Health, USA).

# 2.12. Statistical Analyses

All data were reported as the average  $\pm$  the standard error of the mean. Material characterization data was acquired using a minimum of 6 technical replicate samples per group, at least 10 replicates for biaxial mechanical testing, and one biological sample with four technical replicates for the cadaveric tissue-material testing. Using Prism (v9.0.0, GraphPad Software LLC, San Diego, CA) and p<0.05, significant differences in material properties were identified using one-way Analysis of Variance (ANOVA), followed by Tukey's test for post-hoc determination of significance.

#### 3. Results

# 3.1. Composite coating characterization

Scanning electron microscopy(SEM) of coated endotracheal tubes with PCL-4APEGA composites are shown in Fig. 1. Samples with a PCL fiber diameter of 8  $\mu m$  yielded the lowest average coefficient of friction in comparison to the other groups, however, there were no significant differences identified (Fig. 1B). In all the 4APEGA groups, there was a uniform coverage of the ETT on the outermost layer, whereas complete embedding of the electrospun PCL fibers within the 4APEGA hydrogels was observed in the middle layer (Fig. 1C and D). Additionally, the SEM micrographs also verified the attachment of the PCL-4APEGA composites to the ETTs in the innermost layer. Adhesion between the PCL-4APEGA coating and ETT was tested in wet conditions to evaluate the strength of the interface (Fig. 1E and F). The fibers with 1  $\mu m$  diameter withstood significantly greater loads than the fibers with 8  $\mu m$  diameter (\*p < 0.05).

Swelling behavior of the composites determines the drug delivery behavior as well as the final weight of the tube once it is placed into the trachea. Fig. 2A shows composites containing 4APEGA-5k having the most rapid swelling equilibrium, with the least water absorption and reaching equilibrium after the first 30 min when compared to composites containing 4APEGA-10k and 4APEGA-20k. In contrast, when compared to composites containing 4APEGA-5k, composites containing 4APEGA-10k have high higher water uptake rate since higher molecular weight leads to an increase in the mesh size and increased water update capacities, with swelling equilibrium achieved after 3 h. Among the 3 different groups of composites evaluated, composites containing 4APEGA-20k was observed to have the highest swelling ratio over time due to the increased molecular weight of the hydrogel. Additionally, as shown in Fig. 2A, significant differences (\*p < 0.05) were observed between the 4APEGA-5k composites containing 1  $\mu m$  and 8  $\mu m$  PCL, whereas significant difference (\*p < 0.05) were observed between the 4APEGA-10k composites containing 1  $\mu m$  and 4  $\mu m$  PCL. The 4PEGA alone samples in all 3 groups also displayed a higher swelling ratio when compared to all 4PPEGA-PLC fiber incorporated composites at 60 and

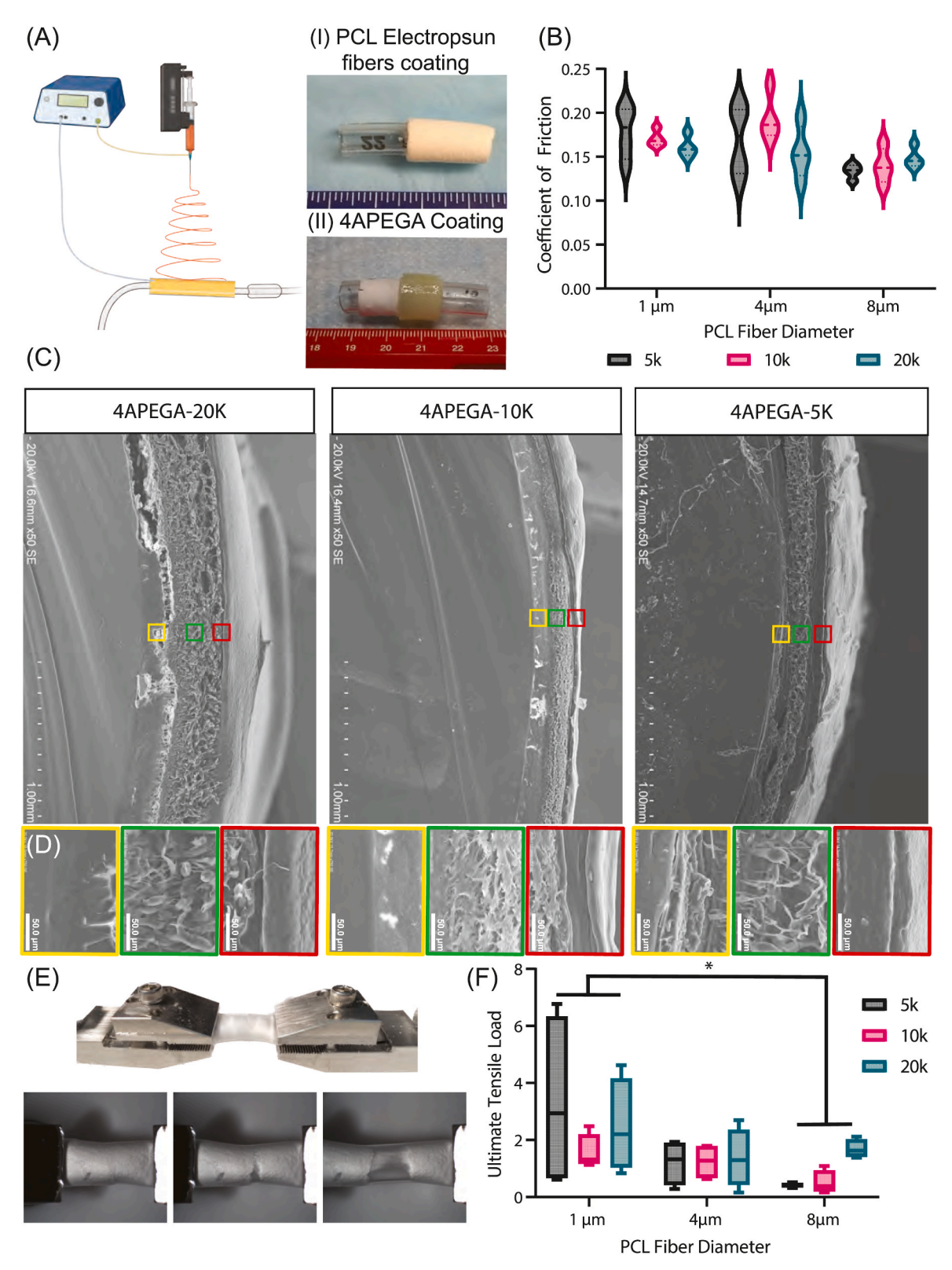


Fig. 1. Morphological Evaluation of PCL-PEGA composite coating on ETTs. (A) A schematic depicting the electrospinning process used in this study. (B) Coefficient of friction for PCL-4APEGA composites (C) Scanning electron microscopy (SEM) showing cross-sections of endotracheal tubes (ETT) coated with PCL-4APEGA composites of different molecular weights (5k, 10k, 20k) and (D) representative high-resolution images of the three regions of interest (ROI), exhibiting uniform coverage of the ETT with 4APEGA in the outermost layer (red ROI), complete embedding of the electrospun PCL fibers within the 4APEGA hydrogels in the middle layer (green ROI), and attachment of the PCL-4APEGA composites to the ETTs in the innermost layer (yellow ROI) of all groups. The scale bars are 1 mm for the gross view and 50  $\mu$ m for the ROIs respectively. (E) Adhesion testing of PCL-4APEGA coating on ETTs and (F) Ultimate tensile load determined from displacement control mode testing. (\* indicates p < 0.05 between groups). (For interpretation of the references to colour in this figure legend, the reader is referred to the Web version of this article.)

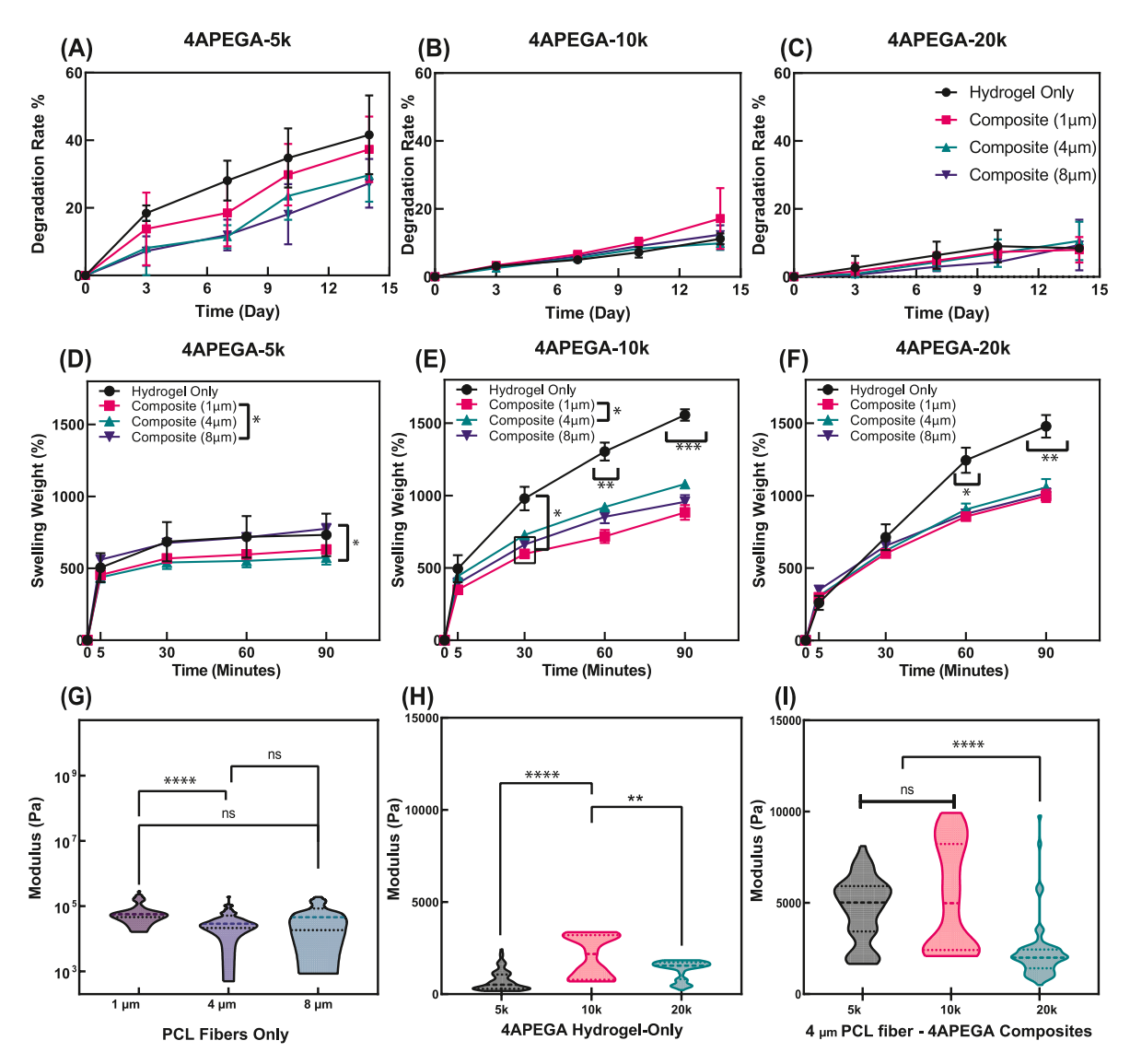


Fig. 2. Structural characterization of 4APEGA. (A, B, and C) Effect of different molecular weights of 4APEGA and the impact of PCL fiber diameter on degradation behavior of 4APEGA hydrogels and the 4APEGA-PCL composites over a period of 14 days. (D, E, and F) Effect of different molecular weights of 4APEGA composites and the impact of PCL fiber diameter on swelling equilibrium over a period of 90 min (G, H, and I) Violin plots with median shown for each column indicating differences in elastic modulus of 1) PCL electrospun fibers with different diameters, 2) 4APEGA-PCL composites of different molecular weights incorporated with 4  $\mu$ m diameter PCL electrospun fibers, and 4APEGA hydrogels with different molecular weights (ns: not significant, \*p < 0.05, \*\*p < 0.01, \*\*\*p < 0.001, \*\*\*\*p < 0.001)

90 min (\*\*p < 0.01 and \*\*\*p < 0.001, respectively).

Fig. 2B shows the degradation properties of composites with 3 different 4APEGA molecular weights and PCL electrospun fibers with different diameters (1, 4, and 8  $\mu m$ ) over 14 days. Overall, degradation of composites with 4APEGA-5k was observed to be relatively higher (41  $\pm$  4 %) compared to composites with 4APEGA-10k or 4APEGA-20k. The degradation rate of composites the 4APEGA-5k was also affected by the diameter of incorporated PCL electrospun fibers, with an increase in degradation (37  $\pm$  4 % for 1  $\mu m$  PCL) observed for composites having smaller fiber diameter. Among the 3 4APEGA groups evaluated, degradation in composites with 4APEGA-20k was observed to be the lowest and the diameter of incorporated PCL in this group has the least impact the degradation behaviors. 4APEGA-10 also demonstrated behavior similar to the 4APEGA-20 composites with fiber diameter having a low impact on composite degradation behavior. The maximum degradation within the 4APEGA-10 and 4APEGA-20 composites was observed in the groups with 1 µm PCL fibers embedded in the hydrogels, which degraded by 17.23  $\pm$  3.74 % and 8.02  $\pm$  1.56 % respectively after 14 days.

Fig. 2G–H shows the elastic modulus of PCL electrospun fibers with different diameters (1, 4, and 8  $\mu m)$  and the impact of hydrogel coating with different molecular weight (5k, 10, 20k) on mechanical properties of the composites. The elastic modulus of 4APEGA hydrogels was observed to be significantly lower when compared to PCL fibers alone and 4APEGA-PCL composites. Although the incorporation of 4  $\mu m$  diameter PCL fibers into 4APEGA composites resulted in an increase in elastic modulus, this increase was not significant when compared to 4APEGA hydrogels. Additionally, while PCL of different molecular weights exhibited significant higher elastic modulus compared to 4APEGA-PCL composites and 4APEGA hydrogels, no differences in elastic modulus was observed between PCL fibers with different diameters.

# 3.2. The impact of ETTs and composites coatings on the inner tracheal lining

Mucus production is generally affected by inflammatory factors including mechanical distress to the epithelial layer [65]. Histology

micrographs at (magnification 4×) (Fig. 3A) stained with Alcian Blue and Fast Red Nucleus to visualized mucus layer, goblet cells, and basement membrane revealing a general disruption in groups in contact with ETT. Goblet cell hyperplasia, epithelial layer abrasion, and tissue compression are prominent features of endotracheal damage to the inner lining of the trachea [66] which is mostly seen in the group in contact with ETT compared to other groups while the tissue group in contact with 4APEGA-5k showed more intact tissue structure after the applied friction. MUC5AC and MUC5B, the predominant mucins in the human airway, have been reported to be significantly increased in response to ventilator-induced lung injuries [67]. Normalized MUC5AC and MUC5B production in tracheal ex-vivo samples in contact with ETT, 4APEGA-5k and 4APEGA-10k, and 4APEGA-20k are shown in Fig. 3B and C. The MUC5AC production (Fig. 3B) decreased in all composite groups after 7 days. MUC5AC production did not change in groups in contact with ETTs between day 1 and 7 while the MUC5AC production decreased significantly in all composite groups compared to ETT group after 7 days. The lowest MUC5AC production was also observed in the tissue groups that are in contact with 4APEGA-5k for 7 days (p < 0.0001). In addition, all composite groups showed significant (p < 0.01) decrease of MUC5AC production at day 7 compared to day 1. MUC5B (Fig. 3C) showed relatively a higher production in all composite groups at day 7 compared to day 1. However, MUC5B secretion was not significantly different between groups.

#### 3.3. Cell adhesion to composite coatings and endotracheal tubes

Cellular adhesion to the endotracheal tube is one of the main indicators of epithelial layer abrasion, followed by inflammation and fibroplasia. Shown in Fig. 4A, Alamar Blue cell adhesion assays indicated a significantly higher hTF adhesion to ETT (18427  $\pm$  837AU)

compared to the 3 groups of 4APEGA hydrogels after 24 h. Among the 4APEGA hydrogels of different molecular weights, 4APEGA-20k hydrogels (2034  $\pm$  112AU) and 4APEGA-5k (12888  $\pm$  1908AU) were observed to have significantly lowest and highest cellular adhesion (p < 0.0001), respectively. As shown in the immunohistochemistry images (Fig. 4B), the attached hTF cells to the tested samples showed confluent cell growth on ETT while the morphology and the number of attached cells was observed to change depending on the molecular weight of the hydrogel, and thus agreeing with the Alamar Blue cell adhesion assays observed in Fig. 4A.

# 3.4. In-vitro dexamethasone release and activity

In-vitro release of dexamethasone from 1 g of PCL electrospun fibers were measured with respect to the different fiber's average diameter (1, 4, and 8 µm) over a period of 24 days. Sustained drug release was exhibited in Fig. 5 for all three concentrations (2.5, 5, and 10 % w:w dexamethasone: PCL), irrespective of fiber's diameter. However, a higher drug release rate was observed for 10 % dexamethasone-loaded PCL fibers of 1  $\mu m$  diameter (0.44  $\pm$  0.003 mg per 1g of PCL) compared to fibers of 4  $\mu m$  (0.24  $\pm$  0.0.006 mg per 1g of PCL) and 8  $\mu m$ diameter (0.094  $\pm$  0.002 mg per 1g of PCL). In addition, it was observed that as the average diameter of PCL electrospun fibers increases, the drug release rate decreased and was less dependent on the initial dexamethasone concentration. The drug release data fitted according to the Korsmeyer-Peppas equation yielded high correlation coefficients  $(R^2 = 0.9919 - 0.9991)$ . Aside from the 8 µm fiber diameter with 2.5 % weight dexamethasone concentration which indicated potential super Case II transport, the n values of Korsmeyer-Peppas remained within 0.45-0.89 indicating anomalous (non-Fickian) diffusion.

Live/dead assay was carried out on samples loaded with

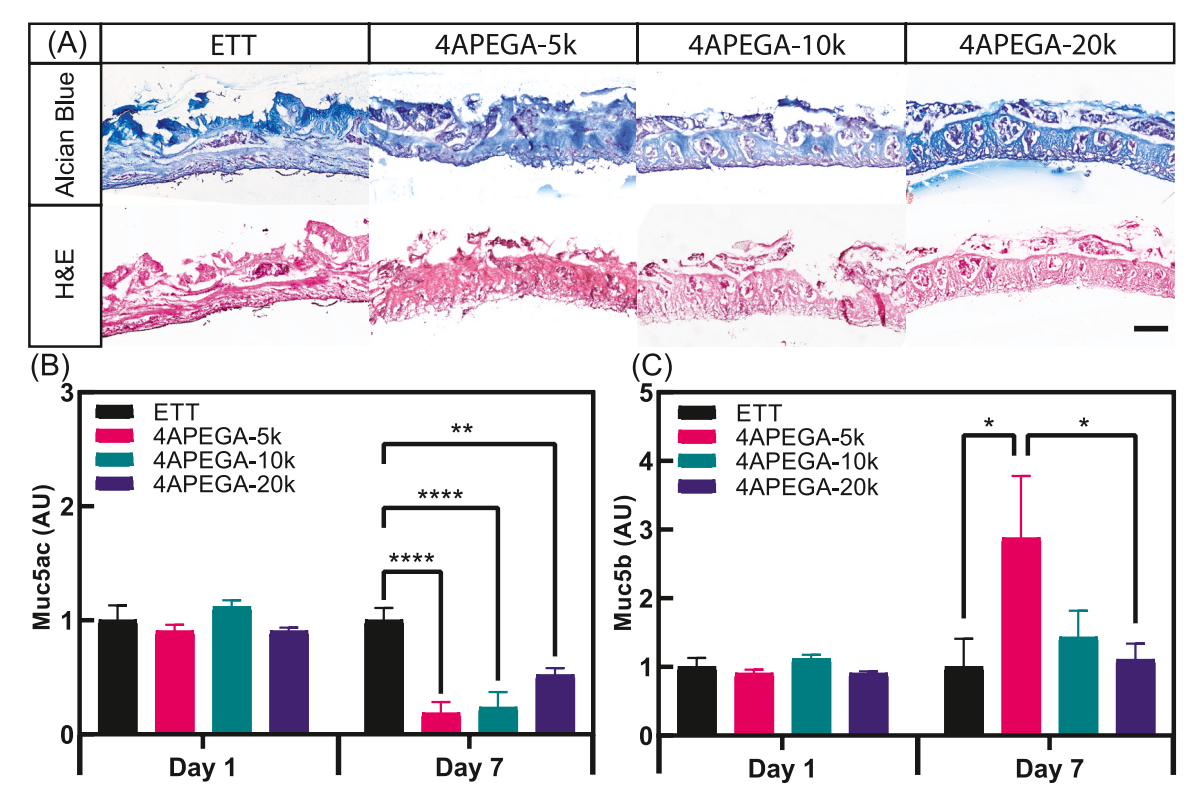


Fig. 3. *Ex-vivo* mucosal damage and mucus production during simulated intubation. (A) Histological evaluation of inner lining of the trachea during simulated intubation using ETT, 4APEGA-5k, 4APEGA-10k, and 4APEGA-20k at days 1 and 7. Tissue samples are stained with Alcian blue and Fast Red Nucleus. (B) Mucus 5AC production from *ex vivo* tissues at days 1 and 7. Data is normalized to ETT muc5ac production. The significant difference (\*p < 0.05) is shown within and between each group. (C) Mucus 5b production from *ex vivo* tissues exposed to ETT, 4APEGA-5k, 4APEGA-10k, and 4APEGA-20k groups at days 1 and 7. The sale bar represents 400  $\mu$ m. (For interpretation of the references to colour in this figure legend, the reader is referred to the Web version of this article.)

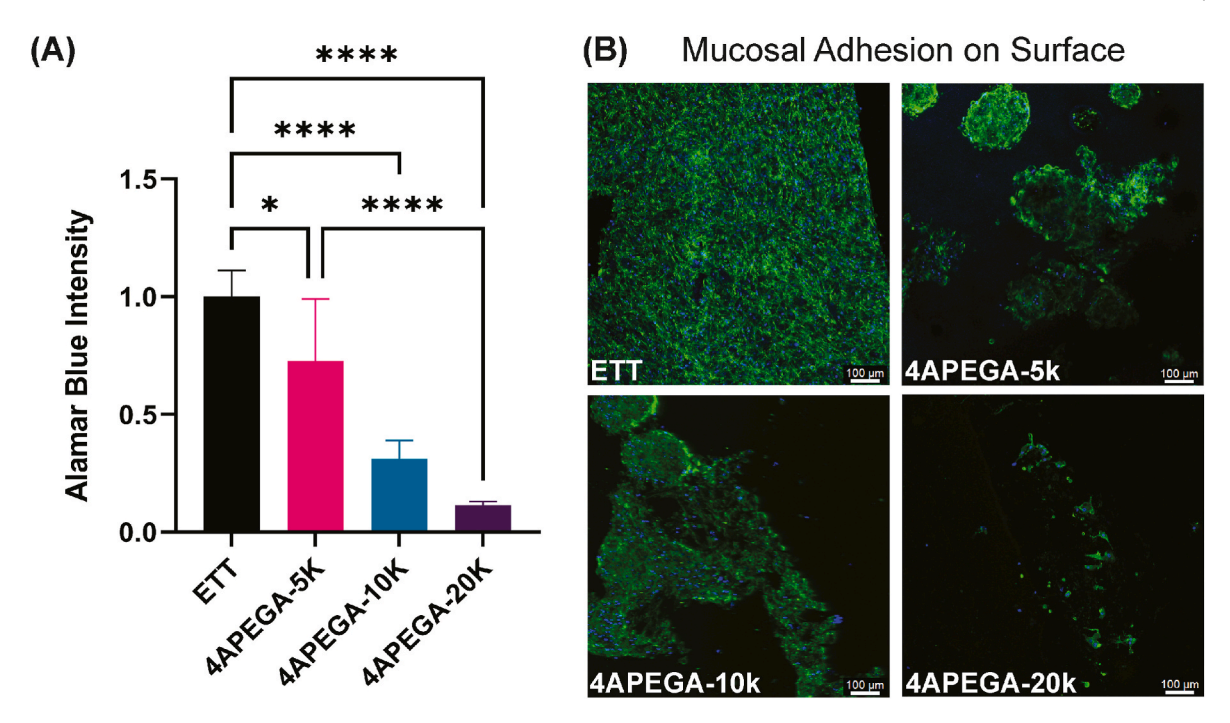


Fig. 4. Cellular Adhesion to the surface of endotracheal tube versus hydrogels after 24 h. (A) Cell adhesion measured by Alamar Blue, with data expressed as the mean and standard error of six independent samples and asterisks indicating P < 0.05. (B) Merged immunohistochemistry images of confocal scanning microscopy showing human tracheal fibroblasts attachment to (1) endotracheal tube, (2) 4APEGA-5k, (3) 4APEGA-10k, and (4) 4APEGA-20k. The scale bar represents 100  $\mu$ m. (For interpretation of the references to colour in this figure legend, the reader is referred to the Web version of this article.)

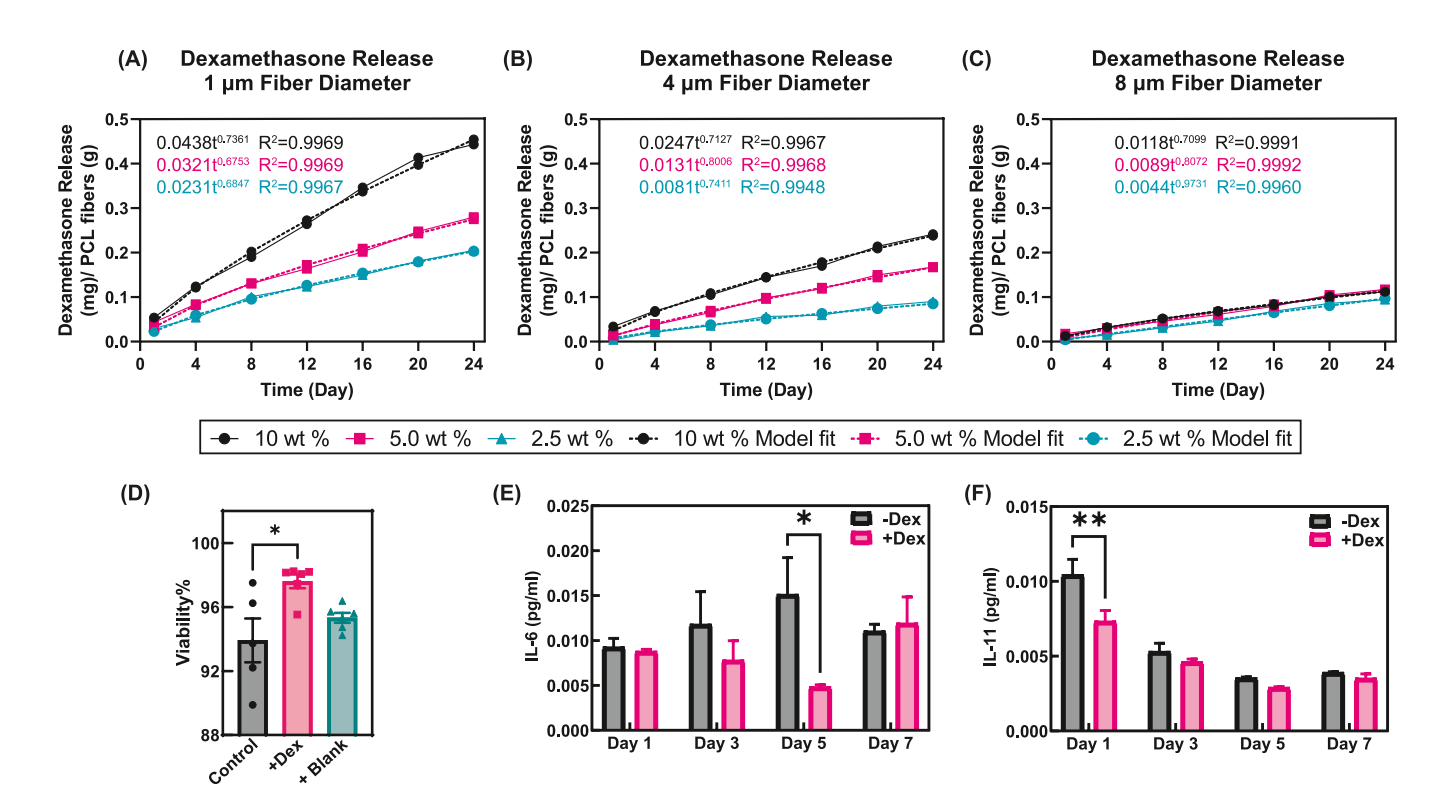


Fig. 5. Released profile of dexamethasone from PCL electrospun fibers, viability, and expression of pro-inflammatory markers over a period of 7 days. (A) Different concentrations of dexamethasone (2.5, 5, and 10 % weight:weight of dexamethasone: PCL) released over a period of 24 days from the electrospun fibers of 1 (A), 4 (B), and 8 (C)  $\mu$ m diameter. The Korsmeyer-Peppas model was fit to describe release kinetics. (D) HTF cell viability at 24 h of incubation after exposure to aliquots collected from different composite groups, indicating dexamethasone-containing eluent exhibiting significantly higher (\*p < 0.05) viability compared to cells exposed to aliquots from the PCL-only group (control). (E) Interlukin-6 (IL-6) expressions in control and dexamethasone-treated groups, with the presence of dexamethasone resulting in significantly lower expressions (\*p < 0.05) compared to controls at day 5. (F) Interlukin-11 expressions over time with the presence of dexamethasone exhibiting significantly lower expressions (\*p < 0.01) compared to the control group at day 1.

dexamethasone only to evaluate the impact of released dexamethasone on the hTF proliferation (Fig. 5D). It was observed that the hTF cells exposed to the dexamethasone containing eluent demonstrated significantly higher cell viability compared to controls (PCL only). Although not significantly different, the control group also exhibited a lower cell viability compared to the blank group (media eluted from fibers not containing dexamethasone).

IL-6 and IL-11 are prominent pro-inflammatory markers produced during fibroplasia. Fig. 5E and F tracks markers produced over 7 days in groups with and without dexamethasone treatment to evaluate the impact of dexamethasone on controlling inflammatory markers in hTF cells in-vitro. The control group (no dexamethasone) exhibited an increase in IL6 secretion in day 5 (0.015  $\pm$  0.002 pg/ml), but this secretion was subsequently decreased in day 7 (0.011  $\pm$  0.0005 pg/ml). Additionally, the level of IL6 secretion in day 5 was significantly higher in the control group compared to the dexamethasone-treated group (0.0057  $\pm$ 0.001 pg/ml). In comparison to IL6 secretions, IL-11 secretion was shown to be significantly higher on day 1, with the control group  $(0.0143 \pm 0.0006 \text{ pg/mol})$  exhibiting significantly higher secretion when compared to the dexamethasone-treated group. Although not significantly different between groups after day 1, IL11 secretions were observed to decrease over time, with the dexamethasone-treated group exhibiting the lowest IL11 secretion (0.0029  $\pm$  0.00005 pg/ml) on day

# 3.5. SiRNA-PEI polyplex release and efficacy

Fig. 6A demonstrates siRNA polyplex released from hydrogels of different molecular weights (5k, 10k, and 20k) at 1, 12, and 24 h at 37 °C. Polyplex released from 4APEGA-5k was relatively higher in the first hour compared to the 4APEGA-10k and 4APEGA-20k. A higher amount (with no significant increase) of polyplex was observed to be released from 4APEGA-10k (41  $\pm$  5 %) and 4APEGA-20k (51  $\pm$  3 %) when compared to polyplex released from 4APEGA-5k (32  $\pm$  2 %) at 24 h.

Shown in Fig. 6B, transfection efficacy and gene silencing properties of polyplex with different n/p ratios (nitrogen to phosphate ratios defined by Equation (1)) were evaluated by testing *smad3* expressed in hTF cells that were exposed to polyplexes, nonsense siRNA, and siRNA-Lipofectamine. The *Smad3* expression was observed to be downregulated when hTF was exposed to polyplex with low n/p values. In comparison to the positive group (siRNA-Lipofectamine), the n/p of 10

was observed to exhibit the highest downregulation compared to the other polyplexes.

At 24 h after treatment, cell toxicity of siRNA and polyplex with different n/p values were evaluated using the Alamar Blue assay. Fig. 6C shows that cells exposed to polyplex with n/p  $\leq$  50 exhibited no significant difference in cell viability when compared to the control group. In contrast, significant decrease in cell viability (p < 0.05) was observed when cells were exposed to polyplex with n/p value higher than 50.

hTF cells exposed to dexamethasone only, siRNA polyplex targeting smad3 only, and dual treatment were stimulated with exogenous recombinant TGF- $\beta$ 1 to study their impact on profibrotic and fibrotic gene expressions. Gene profiling is reported as a clustergram of associated 44 genes in Fig. 7. Knockdown efficacy of smad3 was observed in both siRNA polyplex targeting smad3 only and dual treatment groups. The dexamethasone treatment was observed to result in a significant shift in transcription of all tested genes except for smad3, IL10, CAV1, TGFBR2, and DCN. However, the dual treatment group showed an altered transcriptional pattern where genes associated with profibrotic, inflammatory, and signal transduction decreased.

### 3.6. Evaluation of composite coatings in-vivo

Localized stiffness comparisons between uncoated (regular) ETT groups and dexamethasone ETT groups have been previously recorded by our group [62]. Therefore, only comparisons between composite ETTs are reported (Fig. 8B). Laryngeal tissue with composite coatings had significantly higher stiffness (22.3  $\pm$  0.692 N/m) than uncoated (17.0  $\pm$  0.757 N/m, p < 0.001) and dexamethasone only (18.2  $\pm$  1.04 N/m, p < 0.001) groups at 3 days. After 7 days of ETT placement, local vocal fold stiffness was significantly less in composite coated groups (19.0  $\pm$  0.583 N/m) than uncoated (24.1  $\pm$  0.680 N/m, p < 0.001) and dexamethasone only ETTs (23.6  $\pm$  0.528 N/m, p < 0.001). At 14 days, the tissue with composite coated ETTs (18.3  $\pm$  0.713 N/m) had significantly reduced stiffness in comparison to uncoated ETTs (23.1  $\pm$  0.725 N/m, p < 0.001). Stiffness outcomes decreased over time for the composite coated groups returning closer to native tissue mechanics after 14 days.

The epithelial thickness was determined based on H&E stained vocal fold cross sections (Fig. 8C and D). Vocal fold tissue had a significantly higher epithelial thickness with composite ETTs than regular ETTs at 3 (45.84  $\pm$  2.06  $\mu m$  vs. 24.04  $\pm$  2.66  $\mu m$ , p < 0.001), 7 (42.3  $\pm$  2.06  $\mu m$  vs. 25.5  $\pm$  1.74  $\mu m$ , p < 0.001), and 14 days (38.9  $\pm$  2.66  $\mu m$  vs. 24.8  $\pm$ 

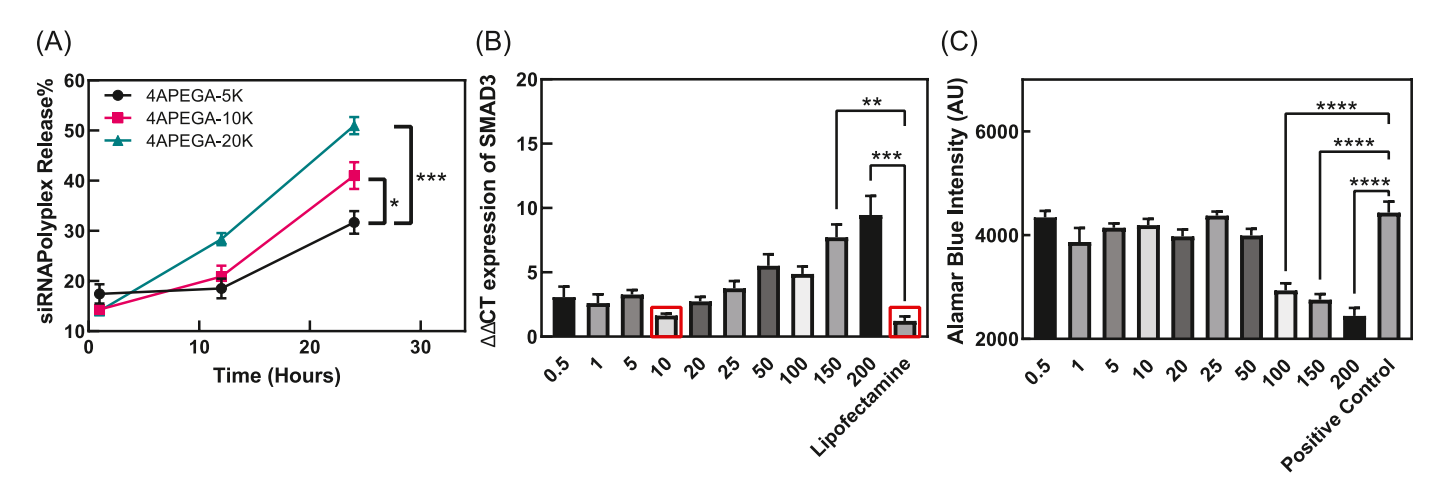


Fig. 6. siRNA Polyplex silencing efficacy, toxicity, and release from the composite. (A) The percentage of siRNA release from 4APEGA-5k, 4APEGA-10k, and 4APEGA-20k hydrogel during 24 h. The polyplex release from 4APEGA-5k was relatively higher in the first hour compared to the 4APEGA-10k and 4APEGA-20k but was the lowest at timepoints 12 and 24 h. At 24 h, the 4APEGA-10k had released  $41 \pm 5$  % of total loaded polyplex and the 4APEGA-20k had released  $51 \pm 3$  % of total loaded polyplex. (B) Silencing efficacy of siRNA polyplex using PEI targeting smad3. Polyplexes with n/p values from 0.5 to 200 and lipofectamine as the control group. The most similar result compared to the positive control group was observed in n/p = 10. (C) Toxicity assay (AlamarBlue) on siRNA polyplex using PEI with n/value 0.5 to 500 reported as arbitrary unit. Significant results are (\*p < 0.05, \*\*p < 0.01, \*\*\*p < 0.001, \*\*\*\*p < 0.0001) between groups.

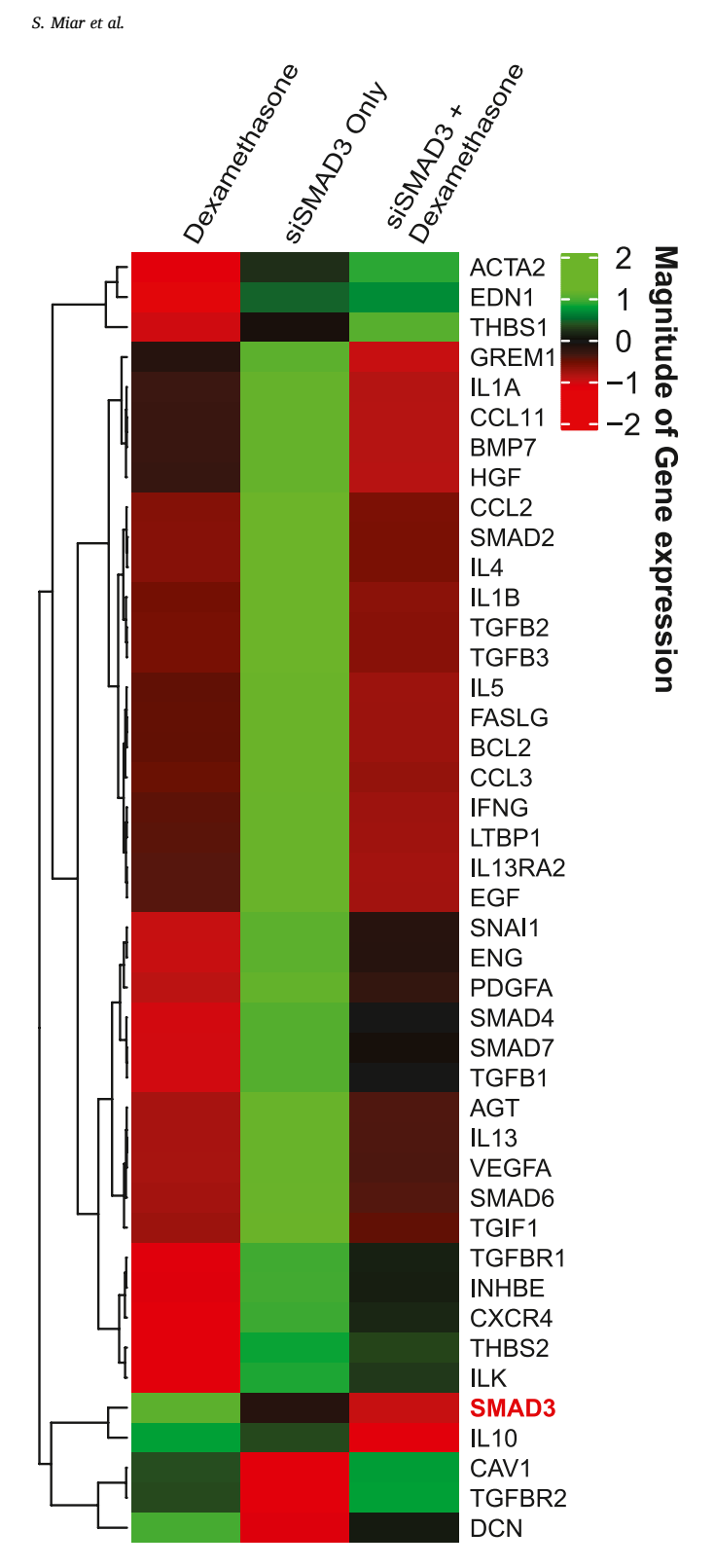


Fig. 7. Clustergram of 44 representative genes exposed to the released dexamethasone, siRNA, and the combination. The expression of mRNA after TGF-β1 stimulation in HTF exposed to dexamethasone only, siRNA polyplex targeting smad3 only, and dual treatment of dexamethasone and siRNA polyplex. The scaled mean of each condition is displayed in the heat map.

3.26  $\mu m$ , p = 0.002). This trend remained similar for comparisons between composite ETTs and dexamethasone only ETTs at 3 (26.8  $\pm$  1.88, p < 0.001), 7 (24.7  $\pm$  4.61  $\mu m$ , p = 0.001), and 14 days (28.8  $\pm$  1.88  $\mu m$ , p = 0.006).

#### 4. Discussion

In this study, the composite coating of PCL electrospun fibers and 4APEGA is developed for its potential as an appropriate endotracheal tube coating to deliver controlled dexamethasone for anti-inflammatory properties and siRNA as an anti-fibrosis therapy. In addition, we demonstrate that the reduction of the general material stiffness using a hydrogel-based composite on the endotracheal tube surface has a direct impact on preserving ex vivo mucosal function, reducing epithelial adhesion, and minimizing epithelial layer abrasion all of which would also potentially allow the coated tube design to prevent the incidence of fibrosis. Our in vivo evaluation demonstrated that 4  $\mu m$  PCL fiber -4APEGA, MW 20k composite endotracheal tubes had reduced vocal fold stiffness and increased epithelial thickness outcomes after 14 days of placement in comparison to the clinical control (uncoated endotracheal tube). More importantly, the stiffness of the vocal fold tissue was seen to return to close to native stiffness levels early and remain at those levels, which is critical for both airway and voice function. We have previously reported that in cases of nerve injury based unilateral dysfunction, the injured vocal fold softens while the contralateral vocal fold overcompensates and stiffens [68,69], while in burn inhalation injured swine, there is increased inflammation and stiffness throughout with intubation [70] compared to native vocal fold stiffness. In the present study, the corticosteroid and siRNA treatment together resulted in the most significant reduction in vocal fold tissue stiffness (and closest to un-injured native stiffness) compared to the uncoated ETT controls after 7 and 14 days post implantation (Fig. 8).

Laryngotracheal stenosis has been reported to be predominantly associated with prolonged endotracheal intubation. The injury is generally initiated with mucosal inflammation, followed by fibroplasia, which leads to progressive airway lumen narrowing [71]. Fibroplasia and scar tissue formation in laryngotracheal stenosis are highly associated with TGF-β1 upregulation and deposition of extracellular matrix (ECM) [59,72]. Most of the recent relevant scholarly literature and current clinical treatment regimen involve investigation or use of systematic (typically steroidal) interventions to suppress fibrosis [73–75], indicating an acute demand for localized treatments of fibroplasia in the affected area. siRNA targeting the SMAD family has been reported to show great potential in downregulating the TGFβ pathway in laryngotracheal stenosis [76,77]. Local drug delivery for siRNA payloads has been previously developed by incorporation in injectable scaffolds [78], direct injection to the affected site [76,77], and loading into scaffolds for different applications [79]; however, due to the practical limitation of access to different parts of laryngotracheal anatomy, especially in intubated patients, a design with localized delivery of biological molecules such as siRNA is essential.

The PEI-siRNA polyplex loaded in the 4APEGA coating developed in the current study has demonstrated the capability to release the siRNA cargo at the topical sites subject to target fibrosis pathway. Drug release profiles observed in 4PEGA coatings determined higher molecular weight facilitate a more rapid siRNA release. This can be due to the increase in mesh size in the polymeric matrix leading to a faster release of polyplex. On the other hand, available carboxylate bonds in 4APEGA hydrogels serve as crosslinking points that cause an electrostatic attraction toward amine groups in cationic PEI of the polyplex. It is suggested from this study that the higher ratio of carboxylate group to PEG chain in 4APEGA-5k compared to 4APEGA with higher molecular weight resulted in higher electrostatic attraction in the matrix between 4APEGA and the polyplex, thereby leading to lower drug release over time. In addition, the smad3 expression results (Fig. 6B) suggest the n/p value of 10 is the optimal polyplex to achieve the highest transfection efficacy and the lowest cell toxicity. Surface chemistry of the coatings also plays an important role for establishing optimal surface lubrication and cell adhesion properties.

There have been multiple reported studies on modified surfaces using mucin-like glycoprotein lubricin to reduce tribological stress and

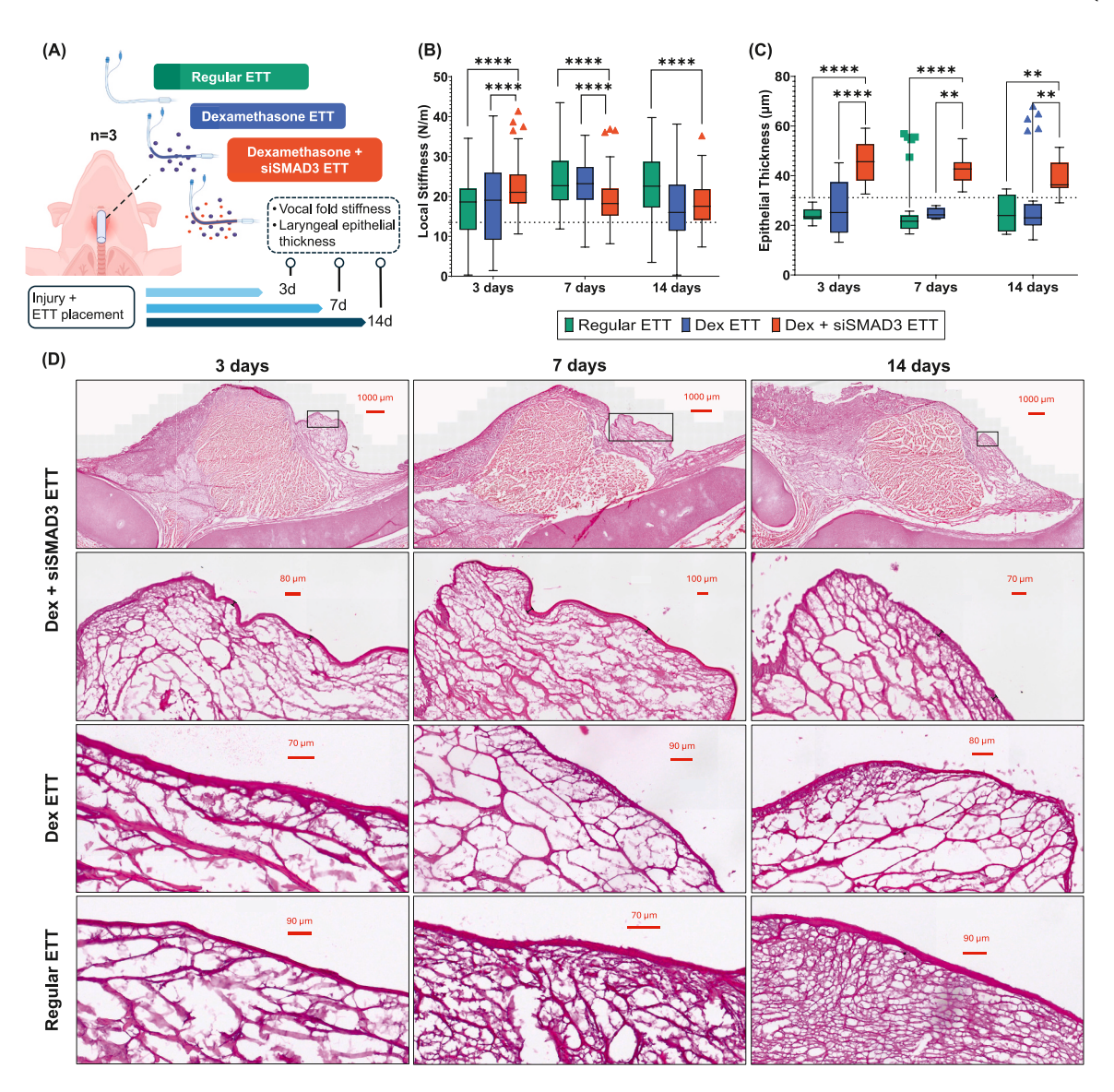


Fig. 8. Traumatic intubation injury simulation and treatment with composite-coated ETTs in swine model (A) Study design; 5 cm segment of uncoated or coated ETTs were placed in an injured airway for 3, 7, and 14 days. (B) Local stiffness (N/m) of vocal fold following injury and placement of composite ETTs. (C) Quantification of epithelial thickness ( $\mu$ m) determined from (D) H&E stained vocal fold sections. Dashed line represents measurements for control larynges without ETT placement or injury (13.5 N/m stiffness and 30.1  $\mu$ m epithelial thickness). Statistically significant differences are indicated by \*<0.05, \*\*<0.01, \*\*\*<0.001, and \*\*\*\*<0.0001.

improve lubricity [80,81]; however, due to the demand of biological resources for mucin production, translation of these biological designs into clinical applications are limited. On the other hand, hydrophilic polymers with neutral charge and hydrogen-bond acceptors have shown the lowest cell adhesion and antifouling properties among the different biomaterials [82]. Due to its low protein absorption rate and neutral nature, PEG is a popular choice for the synthesis of biocompatible coatings [39,83]. 4APEGA is a modified version of the PEG family and is itself a relatively neutral polymer used in this study to form a 3D matrix phase in the composite coating on ETTs. In this study, we demonstrated 4PEGA coatings have significantly lower cell adhesion and water uptake capacities at higher molecular weight, respectively. Secreted mainly by goblet cells, Mucin 5AC is an oligomeric mucus protein predicted to also be an ECM constituent, which is directly affected by the epithelial layer abrasion during intubation (Fig. 3). Damage to the goblet cells has been reported to compromise the protective role of this mucosal barrier against viral and bacterial infections [84]. Mucin5b, a secretion primarily by submucosal glands and submucosal gland ducts, has also been also reported to play a critical role in infection and inflammation

suppression [85,86]. Therefore, modifications of ETTs will prevent the damage to the cells associated with mucus production, resulting in the protection of mucus-coated barriers. Primary human epithelia tissues have been used as ex vivo microphysiological models for a variety of pharmaceutical studies, with the median duration being for eight days and the longest reported study being for 60 days using dynamic physiological culture conditions [87]. We developed the ex vivo bioreactor model based on ex vivo microphysiological models of the pulmonary epithelium used to determine immunological and pharmaceutical responses [88-91]. The mean evaluation period for these systems was 3-7 days [92] which drove the decision to evaluate mucosal secretory response in the laryngotracheal mucosa ex vivo over a 7 day period in the current study when subjected to mechanical abrasion. A recent report details the methods for the ex vivo culture maintenance and mucus production function of the rat tracheal mucosa and indicates that the secretory function of the submucosal gland from the pristine mucosa is maintained in ex vivo culture for over 21 days in a reproducible manner [93]. While 4APEGA offers benefits in terms of preventing epithelium abrasion and rapid drug delivery capabilities, the risk of hydrogel

delamination remains. PCL electrospun fibers as the substrate offers the support required for the stability and reinforcement of the 4APEGA and composite adhesion to ETTs (Fig. 1). In addition, they allow the development of a dual release system directly to the inner epithelial lining of the trachea.

Corticosteroids are highly effective in controlling inflammation but are clinically administered systemically or by injection to lesions. Multiple previous studies have reported methods of incorporating steroids including solid coating [35] and fibers [31,94] to cover endotracheal tube for localized drug delivery. The electrospun fibers used previously were made from poly-lactic-co-glycolic acid (PLGA) and the drug incorporated was another corticosteroid, mometasone furoate [31]. Electrospun fibers have two concerns with exacerbating the local tissue inflammation - the roughness due to the fibers themselves, and in the case of polymers like PLGA, potentially the acidic degradation byproducts of the fibers themselves. This was observed in a successive report from the same group [33], where the PLGA fibers without steroid result in greater mucosal fibrosis than the bare ETT, which is recovered by the delivery of the corticosteroid, but the delivery of the corticosteroid provides no further benefit compared to the bare ETT in a rat model over 1 week of intubation. Within the composite system designed in this study, we attempted to overcome the roughness of the fibers by coating the surface with the 4APEGA and implemented a PCL system to avoid degradation by-products. Similar to the phlorotannin coating that was developed with the intent to specifically prevent fibrosis by targeting the TGFβ signaling [35], we demonstrate the same effect by silencing *smad3*, a core transcription factor of the TGF $\beta$  pathway. We selected to employ 4 μm PCL fiber - 4APEGA, MW 20k composite ETTs in the in vivo study due to the optimal drug release, decreased cellular adhesion, and mucosal damage observed from our in vitro investigation. In our assessment of epithelial thickness after 3, 7, and 14 days of ETT placement in a swine airway injured by epithelial abrasion to mimic intubation injuries, we found the composite ETT with both dexamethasone and smad3 siRNA delivery actually resulted in significantly increased epithelial thickness in comparison to the bare ETT and corticosteroid only ETT. These data indicate that the ex vivo bioreactor model and in vitro responsive cell-based assays were mostly demonstrated to be well correlated across the treatment groups in the large animal preclinical study as well.

Endotracheal intubation also causes vocal fold damage due to the clasping movement between vocal fold and the tube as well as the applied pressure to the vocal cord during the intubation and extubation [95]. It is believed that a soft and lubricated surface reduces mechanical damages to the soft tissue [96]. Hydrogels, as highly water absorbable polymers, have been widely used in self-lubricating designs due to their adjustable tribological behavior [48]. In this study, by using PEG-based hydrogels as the contact layer with inner lining of the trachea, we were aiming to reduce surface stiffness at contact and provide protection for epithelial layer against contacting stiff endotracheal tube surface by interjecting a swellable hydrogel coating. The assessment of elastic modulus confirmed that 4PEGA was substantially less stiff in comparison to PCL electrospun fibers alone and thus may prevent cellular abrasion and further damage that impedes mechanical function. To validate these assumptions, we evaluated the vocal fold stiffness after bare ETT and composite ETT placement in the swine injured airway and found that coated ETTs resulted in a greater local stiffness outcomes at 3 days in comparison to uncoated ETTs. However, over time coated ETTs had reduced local stiffness closer to native tissue properties.

Biofilm production remains a challenging issue in patients with prolonged intubation and systemic steroid administration [97,98], and thus, a different approach of delivering steroid in a sustained-release manner will be required to avoid biofilm production. Multiple commercial ETTs currently incorporate or have applied for regulatory approval to incorporate antimicrobial features including the incorporation of silver, gold, palladium or anti-microbial peptides (ceragenin) and surface texturing to prevent biofilm adhesion [25]. Any of these

methods treating the inner lumen could be paired with the currently developed composite coating on the outer surface of the ETTs. Antimicrobial molecules especially have been broadly studied to prevent and disrupt biofilm formation, including CSA131 in a hydrogel film [27], silver sulfadiazine/chlorohexidine in polyurethane [38], allicin incorporated in a polydopamine coating [34], BCP3 a styrylbenzene based antimicrobial incorporated within PLGA [29] and Lasioglossin-III (Lasio) and A4K14-citropin 1.1 (Citropin) incorporated within PLGA as well [24,32]. A majority of these methods involve the dip coating of the polymer solution containing the anti-microbial on the ETT surface controlled by duration of dip coating, and have all demonstrated not only anti-microbial properties, but local inflammatory control stemming from modulation of the local microbiome when evaluated in vivo. The PCL-4APEGA coating is amenable to including such antimicrobials within either layer of the composite based on intended residence time of the drug.

Small molecule delivery in the upper airway can be challenging due to the complex anatomy and rapid clearance mechanisms of the respiratory system. To achieve effective drug delivery, it is important to optimize the residence time of the drug in the upper airway. The use of siRNA-PEI polyplexes complexed with 4APEGA as a drug carrier and depot represented a promising approach for targeted delivery of siRNA molecules to the upper airway. The siRNA-PEI polyplexes can protect the siRNA from degradation and facilitate uptake by the target cells, while the 4APEGA hydrogel can provide sustained release of the polyplex, leading to prolonged and controlled inhibition of the SMAD3 pathway. Furthermore, the use of 4APEGA- PCL composite as a coating for ETTs allows for flexibility in the types of payloads that can be delivered using this system, potentially allowing for broader clinical use. This study has demonstrated that PCL electrospun fibers can be successfully embedded in 4APEGA hydrogels as well as having dexamethasone released through the composite without exposing the PCL fibers to the inner lining of the trachea. The drug release mechanism from PCL fibers is controlled by solid-state diffusion, rather than by chemical or swelling factors [99] while the drug release from 4APEGA is controlled mainly by swelling factors. This assisted us to leverage from a dual phase release of small molecules from the composites to target different inflammation pathways. Furthermore, since we employ volumetric coatings, the limit on therapeutic loading is not limited as in the case of direct tethering of drug to the surface of the ETTs or the tethering of nanoparticles encapsulating the drug to the functionalized ETT surface [40].

# 5. Conclusion

In this study, a novel approach was introduced for the modification of ETTs through the development and thorough characterization of PCL-4APEGA composite coating. This composite coating exhibited dual drug delivery capabilities, showcasing its potential in equipping ETTs with tunable drug delivery potentials. A significant reduction in stiffness of the contact surface and ability to provide hydrogel coating-based protection to the epithelial mucosa against an otherwise stiff and abrasive endotracheal tube surface was demonstrated in an ex vivo model. Furthermore, the incorporation of electrospun PCL fibers within the 4APEGA hydrogels proved to be an effective platform for tunable dexamethasone delivery as an anti-inflammatory agent. Additionally, the study highlighted the composite coating's capacity for local drug delivery of siRNA polyplexes from the 4APEGA matrix in the first 24 h to address fibrosis and inflammation in the context of endotracheal intubation. To improve the bioavailability of siRNA, PEI was used as a siRNA carrier and carrier:siRNA ratio optimization was carried out to yield the highest transfection efficacy while minimizing cell toxicity. In conclusion, the findings from this study offer comprehensive evidence that the novel PCL-4APEGA-coated ETT represents a promising and mucosacompatible platform for drug delivery from ETTs. This technology has the potential to not only minimize the occurrence of focal airway

damage during intubation but also modulate the inflammatory and fibrotic responses through multimodal, controlled, and localized drug delivery. The innovative approach presented in this study has the potential to significantly improve the safety and efficacy of endotracheal tubes and ultimately enhance patient outcomes in critical care settings.

# CRediT authorship contribution statement

Solaleh Miar: Writing – review & editing, Writing – original draft, Validation, Formal analysis, Data curation, Investigation, Visualization. Gabriela Gonzales: Writing – review & editing, Methodology, Data curation, Conceptualization. Gregory Dion: Writing – review & editing, Writing – original draft, Supervision, Project administration, Methodology, Funding acquisition, Conceptualization. Joo L. Ong: Writing – review & editing, Resources, Methodology, Funding acquisition, Conceptualization. Ronit Malka: Methodology, Writing – review & editing, Data curation. Rena Bizios: Writing – review & editing, Resources, Methodology, Formal analysis, Data curation, Conceptualization. Teja Guda: Writing - original draft, Writing - review & editing, Methodology, Formal analysis, Funding Acquisition, Data curation, Conceptualization.

# Declaration of competing interest

The authors declare the following financial interests/personal relationships which may be considered as potential competing interests: Teja Guda reports financial support was provided by 59MDW Office of the Chief Scientist. Teja Guda has patent pending to UT System Board of Regents.

#### Data availability

Data will be made available on request.

### 6. Acknowledgments

T. Guda, R. Bizios and J. L. Ong are supported by the University of Texas at San Antonio through the Jacobson endowment, the Lutcher Brown endowment and the USAAFoundation endowment respectively. T. Guda was supported in part by the National Science Foundation through grant number 1847103. The U.S. Department of Defense through the 59MDW/Office of the Chief Scientist Office sponsored S. Miar, G. R. Dion and T. Guda through grant funding (AC20COV10 and AC19EC06) to support in part technology developed in this manuscript. There is no commercial interest or industry funding to any of the authors regarding any material discussed in this manuscript.

# Appendix A. Supplementary data

Supplementary data to this article can be found online at https://doi.org/10.1016/j.biomaterials.2024.122602.

# References

- [1] A.T. Hillel, S. Karatayli-Ozgursoy, I. Samad, S.R. Best, V. Pandian, L. Giraldez, J. Gross, C. Wootten, A. Gelbard, L.M. Akst, M.M. Johns, C. North American Airway, Predictors of posterior glottic stenosis: a multi-institutional case-control study, Ann. Otol. Rhinol. Laryngol. 125 (3) (2016) 257–263.
- [2] N.G. Katsantonis, E.K. Kabagambe, C.T. Wootten, E.W. Ely, D.O. Francis, A. Gelbard, Height is an independent risk factor for postintubation laryngeal injury, Laryngoscope 128 (12) (2018) 2811–2814.
- [3] J.A. Koufman, J.K. Fortson, M.S. Strong, Predictive factors of cricoid ring size in adults in relation to acquired subglottic stenosis, Otolaryngol. Head Neck Surg. 91 (2) (1983) 177–182.
- [4] Y. Lahav, H. Shoffel-Havakuk, D. Halperin, Acquired glottic stenosis-the Ongoing challenge: a review of etiology, pathogenesis, and surgical management, J. Voice 29 (5) (2015) 646 e1–e646 e10.

[5] S. Pookamala, A. Thakar, K. Puri, P. Singh, R. Kumar, S.C. Sharma, Acquired subglottic stenosis: aetiological profile and treatment results, J. Laryngol. Otol. 128 (7) (2014) 641–648.

- [6] R.E. Whited, Laryngeal dysfunction following prolonged intubation, Ann. Otol. Rhinol. Laryngol. 88 (4 Pt 1) (1979) 474–478.
- [7] J.R. Shinn, K.S. Kimura, B.R. Campbell, A. Sun Lowery, C.T. Wootten, C.G. Garrett, D.O. Francis, A.T. Hillel, L. Du, J.D. Casey, E.W. Ely, A. Gelbard, Incidence and outcomes of acute laryngeal injury after prolonged mechanical ventilation, Crit. Care Med. 47 (12) (2019) 1699–1706.
- [8] N.K. Adhikari, R.A. Fowler, S. Bhagwanjee, G.D. Rubenfeld, Critical care and the global burden of critical illness in adults, Lancet 376 (9749) (2010) 1339–1346.
- [9] A.J. Neevel, J.D. Smith, R.J. Morrison, N.D. Hogikyan, R.A. Kupfer, A.P. Stein, Postacute COVID-19 laryngeal injury and dysfunction, OTO Open 5 (3) (2021), 2473974x211041040.
- [10] S.A. Nouraei, A. Singh, A. Patel, C. Ferguson, D.J. Howard, G.S. Sandhu, Early endoscopic treatment of acute inflammatory airway lesions improves the outcome of postintubation airway stenosis, Laryngoscope 116 (8) (2006) 1417–1421.
- [11] A.N. Hollis, A. Ghodke, D. Farquhar, R.A. Buckmire, R.N. Shah, Postoperative inhaled steroids following glottic airway surgery reduces granulation tissue formation, Ann. Otol. Rhinol. Laryngol. 131 (11) (2022) 1267–1273.
- [12] C. Kremer, R. Jiang, A. Singh, J. Sukys, A. Brackett, N. Kohli, Factors affecting posterior glottic stenosis surgery outcomes: systematic review and meta-analysis, Ann. Otol. Rhinol. Laryngol. 130 (10) (2021) 1156–1163.
- [13] S.J. Rao, G.E. Gochman, A. Stasyuk, K.L. Del Rosario, D.J. Cates, L.L. Madden, V. N. Young, Interventions and outcomes in glottic versus multi-level airway stenosis: a multi-institutional review, Laryngoscope 133 (3) (2023) 528–534.
- [14] R.A. Franco Jr., I. Husain, L. Reder, P. Paddle, Awake serial intralesional steroid injections without surgery as a novel targeted treatment for idiopathic subglottic stenosis, Laryngoscope 128 (3) (2018) 610–617.
- [15] M.R. Hoffman, A.R. Coughlin, S.H. Dailey, Serial office-based steroid injections for treatment of idiopathic subglottic stenosis, Laryngoscope 127 (11) (2017) 2475–2481.
- [16] M. Wierzbicka, M. Tokarski, M. Puszczewicz, W. Szyfter, The efficacy of submucosal corticosteroid injection and dilatation in subglottic stenosis of different aetiology, J. Laryngol. Otol. 130 (7) (2016) 674–679.
- [17] C. Bertelsen, H. Shoffel-Havakuk, K. O'Dell, M.M. Johns 3rd, L.S. Reder, Serial inoffice intralesional steroid injections in airway stenosis, JAMA Otolaryngol Head Neck Surg 144 (3) (2018) 203–210.
- [18] Y.-P. Li, W. Liu, Y.-H. Liu, Y. Ren, Z.-G. Wang, B. Zhao, S. Huang, J.-Z. Xu, Z.-M. Li, Highly improved aqueous lubrication of polymer surface by noncovalently bonding hyaluronic acid-based hydration layer for endotracheal intubation, Biomaterials 262 (2020) 120336.
- [19] B. Zhao, Y.-P. Li, Q. Wang, Y. Ren, Z.-L. Zheng, M.-H. Bai, J.-C. Lv, K. Li, J.-Z. Xu, Z.-M. Li, X. Song, Ultra-slippery, nonirritating, and anti-inflammatory hyaluronic acid-based coating to mitigate intubation injury, Chem. Eng. J. 427 (2022) 130911.
- [20] S. Malli, C. Bories, B. Pradines, P.M. Loiseau, G. Ponchel, K. Bouchemal, In situ forming pluronic® F127/chitosan hydrogel limits metronidazole transmucosal absorption, Eur. J. Pharm. Biopharm. 112 (2017) 143–147.
- [21] N. Hiwatashi, P.A. Benedict, G.R. Dion, R. Bing, I. Kraja, M.R. Amin, R.C. Branski, SMAD3 expression and regulation of fibroplasia in vocal fold injury, Laryngoscope 127 (9) (2017) F308–e316
- [22] J. Lu, W. Tian, L. Cui, B. Cai, T. Zhang, N. Huang, L. Lu, T. Zhu, Lidocaine-eluting endotracheal tube effectively attenuates intubation related airway response, Ann. Transl. Med. 9 (10) (2021) 871.
- [23] H. Yu, Q. Chu, J. Liu, L. Chen, Y. Wang, Y. Zuo, EMLA® cream coated on endotracheal tube with or without epidural lidocaine reduces isoflurane requirement during general anesthesia, Front. Med. 6 (3) (2012) 302–306.
- [24] M.R. Aronson, S. Ali Akbari Ghavimi, P.M. Gehret, I.N. Jacobs, R. Gottardi, Drugeluting endotracheal tubes for preventing bacterial inflammation in subglottic stenosis, Laryngoscope 132 (7) (2022) 1356–1363.
- [25] M. Barnes, C. Feit, T.-A. Grant, E.J. Brisbois, Antimicrobial polymer modifications to reduce microbial bioburden on endotracheal tubes and ventilator associated pneumonia, Acta Biomater. 91 (2019) 220–234.
- [26] L. Berra, F. Curto, G. Li Bassi, P. Laquerriere, B. Pitts, A. Baccarelli, T. Kolobow, Antimicrobial-coated endotracheal tubes: an experimental study, Intensive Care Med. 34 (6) (2008) 1020–1029.
- [27] M.M. Hashemi, J. Rovig, J. Bateman, B.S. Holden, T. Modelzelewski, I. Gueorguieva, M. von Dyck, R. Bracken, C. Genberg, S. Deng, P.B. Savage, Preclinical testing of a broad-spectrum antimicrobial endotracheal tube coated with an innate immune synthetic mimic, J. Antimicrob. Chemother. 73 (1) (2018) 143–150.
- [28] C.-c. Hu, Y. Yu, H.-l. Qian, Y.-f. Chen, L.-y. Zou, C.-m. Zhang, K.-f. Ren, Z.-h. Yang, J. Ji, Antibacterial endotracheal tube with silver-containing double-network hydrogel coating, Colloid and Interface Science Communications 55 (2023) 100724.
- [29] B. Ozcelik, P. Pasic, P. Sangwan, C.L. Be, V. Glattauer, H. Thissen, R.A. Boulos, Evaluation of the novel antimicrobial BCP3 in a coating for endotracheal tubes, ACS Omega 5 (18) (2020) 10288–10296.
- [30] Y. Wang, B. Cai, D. Ni, Y. Sun, G. Wang, H. Jiang, A novel antibacterial and antifouling nanocomposite coated endotracheal tube to prevent ventilatorassociated pneumonia, J. Nanobiotechnol. 20 (1) (2022) 112.
- [31] A. Abu Ammar, M. Gruber, P. Martin, O. Stern, F. Jahshan, O. Ertracht, E. Sela, S. Srouji, E. Zussman, Local delivery of mometasone furoate from an eluting endotracheal tube, J. Contr. Release 272 (2018) 54–61.
- [32] M.R. Aronson, A. Mehta, R.M. Friedman, D.D. Ghaderi, R.C. Borek, H.C.B. Nguyen, K.S. McDaid, I.N. Jacobs, N. Mirza, R. Gottardi, Amelioration of Subglottic Stenosis

- by Antimicrobial Peptide Eluting Endotracheal Tubes, Cellular and Molecular Bioengineering, 2023.
- [33] F. Jahshan, A. Abu Ammar, O. Ertracht, N. Eisenbach, A. Daoud, E. Sela, S. Atar, E. Zussman, B. Fichtman, A. Harel, M. Gruber, Local delivery of mometasone furoate from an eluting endotracheal tube reduces airway morbidity following long-term animal intubation, ACS Appl. Bio Mater. 4 (5) (2021) 4131–4139.
- [34] H. Jung, J.S. Lee, J.J. Lee, H.S. Park, Anti-inflammatory and anti-bacterial effects of allicin-coated tracheal tube on trachea mucosa 36 (3) (2022) 1195.
- [35] H.S. Lee, M.S. Jeong, S.C. Ko, S.Y. Heo, H.W. Kang, S.W. Kim, C.W. Hwang, K. D. Lee, C. Oak, M.J. Jung, Fabrication and biological activity of polycaprolactone/phlorotannin endotracheal tube to prevent tracheal stenosis: an in vitro and in vivo study, J. Biomed. Mater. Res. B Appl. Biomater. 108 (3) (2020) 1046–1056.
- [36] D. Alves, T. Grainha, M.O. Pereira, S.P. Lopes, Antimicrobial materials for endotracheal tubes: a review on the last two decades of technological progress, Acta Biomater. 158 (2023) 32–55.
- [37] L. Marcut, V. Manescu, A. Antoniac, G. Paltanea, A. Robu, A.G. Mohan, E. Grosu, I. Corneschi, A.D. Bodog, Antimicrobial solutions for endotracheal tubes in prevention of ventilator-associated pneumonia, Materials 16 (14) (2023) 5034.
- [38] L. Berra, L. De Marchi, Z.-X. Yu, P. Laquerriere, A. Baccarelli, T. Kolobow, Endotracheal tubes coated with antiseptics decrease bacterial colonization of the ventilator circuits, lungs, and endotracheal tube, Anesthesiology 100 (6) (2004) 1446–1456.
- [39] B. Ozcelik, K.K.K. Ho, V. Glattauer, M. Willcox, N. Kumar, H. Thissen, Poly (ethylene glycol)-based coatings combining low-biofouling and quorum-sensing inhibiting properties to reduce bacterial colonization, ACS Biomater. Sci. Eng. 3 (1) (2017) 78–87.
- [40] J. Mokkaphan, W. Banlunara, T. Palaga, P. Sombuntham, S. Wanichwecharungruang, Silicone surface with drug nanodepots for medical devices, ACS Appl. Mater. Interfaces 6 (22) (2014) 20188–20196.
- [41] C.M. Johnson, A.S. Luke, C. Jacobsen, N. Novak, G.R. Dion, State of the science in tracheal stents: a scoping review, Laryngoscope 132 (11) (2022) 2111–2123.
- [42] J. Barthes, P. Lagarrigue, V. Riabov, G. Lutzweiler, J. Kirsch, C. Muller, E. J. Courtial, C. Marquette, F. Projetti, J. Kzhyskowska, P. Lavalle, N.E. Vrana, A. Dupret-Bories, Biofunctionalization of 3D-printed silicone implants with immunomodulatory hydrogels for controlling the innate immune response: an in vivo model of tracheal defect repair, Biomaterials 268 (2021) 120549.
- [43] S.J. Lee, J.S. Choi, M.R. Eom, H.H. Jo, I.K. Kwon, S.K. Kwon, S.A. Park, Dexamethasone loaded bilayered 3D tubular scaffold reduces restenosis at the anastomotic site of tracheal replacement: in vitro and in vivo assessments, Nanoscale 12 (8) (2020) 4846–4858.
- [44] J.S. Choi, J.M. Kim, J.W. Kim, Y.M. Kim, I.S. Park, S.G. Yang, Prevention of tracheal inflammation and fibrosis using nitinol stent coated with doxycycline, Laryngoscope 128 (7) (2018) 1558–1563.
- [45] Y. Li, M. Li, X. Wang, Y. Wang, C. Li, Y. Zhao, Z. Li, J. Chen, J. Li, K. Ren, X. Duan, J. Ren, X. Han, Q. Li, Arsenic trioxide-eluting electrospun nanofiber-covered self-expandable metallic stent reduces granulation tissue hyperplasia in rabbit trachea, Biomedical Materials 16 (1) (2021) 015013.
- [46] S. Ali Akbari Ghavimi, P.M. Gehret, M.R. Aronson, R. Schipani, K.W.Y. Smith, R. C. Borek, J.A. Germiller, I.N. Jacobs, K.B. Zur, R. Gottardi, Drug delivery to the pediatric upper airway, Adv. Drug Deliv. Rev. 174 (2021) 168–189.
- [47] P. Zarogoulidis, K. Sapalidis, C. Kosmidis, K. Tsakiridis, H. Huang, C. Bai, W. Hohenforst-Schmidt, S. Tryfon, A. Vagionas, K. Drevelegas, E.-I. Perdikouri, L. Freitag, Stents for small airways: current practice, Expet Rev. Respir. Med. 14 (10) (2020) 969–972.
- [48] J.P. Gong, Friction and lubrication of hydrogels—its richness and complexity, Soft Matter 2 (7) (2006) 544–552.
- [49] B.R. Machado, S.B. Roberto, E.G. Bonafé, S.E. Camargo, C.H. Camargo, K.C. Popat, M.J. Kipper, A.F. Martins, Chitosan imparts better biological properties for poly (\varepsilon-caprolactone) electrospun membranes than dexamethasone, J. Braz. Chem. Soc. 30 (8) (2019) 1741–1750.
- [50] J.D. Ziebarth, Y. Wang, Understanding the protonation behavior of linear polyethylenimine in solutions through Monte Carlo simulations, Biomacromolecules 11 (1) (2010) 29–38.
- [51] D.C. Arruda, C. Hoffmann, C. Charrueau, P. Bigey, V. Escriou, Innovative nonviral vectors for small-interfering RNA delivery and therapy, Nanostructures for Novel Therapy (2017) 713–740. Elsevier.
- [52] H.R. Kim, I.K. Kim, K.H. Bae, S.H. Lee, Y. Lee, T.G. Park, Cationic solid lipid nanoparticles reconstituted from low density lipoprotein components for delivery of siRNA, Mol. Pharm. 5 (4) (2008) 622–631.
- [53] S.H. Lee, H. Mok, Y. Lee, T.G. Park, Self-assembled siRNA-PLGA conjugate micelles for gene silencing, J. Contr. Release 152 (1) (2011) 152-158.
- [54] S. Patil, R. Lalani, P. Bhatt, I. Vhora, V. Patel, H. Patel, A. Misra, Hydroxyethyl substituted linear polyethylenimine for safe and efficient delivery of siRNA therapeutics, RSC advances 8 (62) (2018) 35461–35473.
- [55] R. Cheraghi, M. Alipour, M. Nazari, S. Hosseinkhani, Optimization of conditions for gene delivery system based on PEI, Nanomedicine Journal 4 (1) (2017) 8–16.
- [56] E. Özgür, N. Bereli, D. Türkmen, S. Ünal, A. Denizli, PHEMA cryogel for in-vitro removal of anti-dsDNA antibodies from SLE plasma, Mater. Sci. Eng. C 31 (5) (2011) 915–920.
- [57] R.W. Korsmeyer, R. Gurny, E. Doelker, P. Buri, N.A. Peppas, Mechanisms of solute release from porous hydrophilic polymers, Int. J. Pharm. 15 (1) (1983) 25–35.
- [58] P. Spaepen, S. De Boodt, J.-M. Aerts, J. Vander Sloten, Digital image processing of live/dead staining, Mammalian Cell Viability (2011) 209–230. Springer.
- [59] N. Hiwatashi, P.A. Benedict, G.R. Dion, R. Bing, I. Kraja, M.R. Amin, R.C. Branski, SMAD 3 expression and regulation of fibroplasia in vocal fold injury, Laryngoscope 127 (9) (2017) E308–E316.

- [60] R.C. Team, R: A Language and Environment for Statistical Computing, 2013.
- [61] Z. Gu, R. Eils, M. Schlesner, Complex heatmaps reveal patterns and correlations in multidimensional genomic data, Bioinformatics 32 (18) (2016) 2847–2849.
- [62] G. Gonzales, R. Malka, L. Marinelli, C.M. Lee, S. Miar, S. Cook, G.R. Dion, T. Guda, Endotracheal tubes with dexamethasone eluting electrospun coating improve tissue mechanical function after upper airway injury, Sci. Rep. 14 (1) (2024) 2821.
- [63] G.R. Dion, T. Guda, S. Mukudai, R. Bing, J.F. Lavoie, R.C. Branski, Quantifying vocal fold wound-healing biomechanical property changes, Laryngoscope 130 (2) (2020) 454–459.
- [64] G.R. Dion, J.F. Lavoie, P. Coelho, M.R. Amin, R.C. Branski, Automated indentation mapping of vocal fold structure and cover properties across species, Laryngoscope 129 (1) (2019) E26–E31.
- [65] J.V. Fahy, B.F. Dickey, Airway mucus function and dysfunction, N. Engl. J. Med. 363 (23) (2010) 2233–2247.
- [66] C.A. Puyo, S.M. Tricomi, T.E. Dahms, Early biochemical markers of inflammation in a swine model of endotracheal intubation, Anesthesiology: The Journal of the American Society of Anesthesiologists 109 (1) (2008) 88–94.
- [67] M. Koeppen, E.N. McNamee, K.S. Brodsky, C.M. Aherne, M. Faigle, G. Downey, S. Colgan, C. Evans, D. Schwartz, H.K. Eltzschig, Detrimental role of the airway mucin Muc5ac during ventilator-induced lung injury, Mucosal Immunol. 6 (4) (2013) 762–775.
- [68] R. Malka, A. Isaac, G. Gonzales, S. Miar, B. Walters, A. Baker, T. Guda, G.R. Dion, Changes in vocal fold gene expression and histology after injection augmentation in a recurrent laryngeal nerve injury model, J. Laryngol. Otol. 138 (2) (2024) 196-202
- [69] S. Miar, G.R. Dion, S. Montelongo, J.L. Ong, R. Bizios, T. Guda, Development of a bioinspired, self-adhering, and drug-eluting laryngotracheal patch, Laryngoscope 131 (19) (2021) 1958–1966.
- [70] R. Malka, G. Gonzales, W. Detar, L. Marinelli, C.M. Lee, A. Isaac, S. Miar, S. Cook, T. Guda, G.R. Dion, Effect of continuous local dexamethasone on tissue biomechanics and histology after inhalational burn in a preclinical model, Laryngoscope Investigative Otolaryngology 8 (4) (2023) 939–945.
- [71] Z. Cai, H. Li, H. Zhang, S. Han, R. An, X. Yan, Novel insights into the role of hypoxia-inducible factor-1 in the pathogenesis of human post-intubation tracheal stenosis, Mol. Med. Rep. 8 (3) (2013) 903–908.
- [72] C. Karagiannidis, V. Velehorschi, B. Obertrifter, H.-N. Macha, A. Linder, L. Freitag, High-level expression of matrix-associated transforming growth factor-β1 in benign airway stenosis, Chest 129 (5) (2006) 1298–1304.
- [73] M.B. Dolovich, R. Dhand, Aerosol drug delivery: developments in device design and clinical use, Lancet 377 (9770) (2011) 1032–1045.
- [74] B.K. Rubin, R.W. Williams, Emerging aerosol drug delivery strategies: from bench to clinic, Adv. Drug Deliv. Rev. 75 (2014) 141–148.
- [75] P. Allen, V.N. Lawrence, Tracheal Intubation Medications, StatPearls Publishing, Treasure Island (FL), 2023.
- [76] R.C. Branski, R. Bing, I. Kraja, M.R. Amin, The role of S mad 3 in the fibrotic phenotype in human vocal fold fibroblasts, Laryngoscope 126 (5) (2016) 1151–1156.
- [77] B.C. Paul, B.Y. Rafii, S. Gandonu, R. Bing, H. Born, M.R. Amin, R.C. Branski, Smad3: an emerging target for vocal fold fibrosis, Laryngoscope 124 (10) (2014) 2327–2331.
- [78] C.E. Nelson, M.K. Gupta, E.J. Adolph, S.A. Guelcher, C.L. Duvall, siRNA delivery from an injectable scaffold for wound therapy, Adv. Wound Care 2 (3) (2013) 93–99.
- [79] M.D. Krebs, E. Alsberg, Localized, targeted, and sustained siRNA delivery, Chemistry 17 (11) (2011) 3054.
- [80] B. Winkeljann, P.M.A. Leipold, O. Lieleg, Macromolecular coatings enhance the tribological performance of polymer-based lubricants, Adv. Mater. Interfac. 6 (16) (2019) 1900366.
- [81] B. Winkeljann, M.G. Bauer, M. Marczynski, T. Rauh, S.A. Sieber, O. Lieleg, Covalent mucin coatings form stable anti-biofouling layers on a broad range of medical polymer materials, Adv. Mater. Interfac. 7 (4) (2020) 1902069.
- [82] A. Pape, B.D. Ippel, P.Y. Dankers, Cell and protein fouling properties of polymeric mixtures containing supramolecular poly (ethylene glycol) additives, Langmuir 33 (16) (2017) 4076–4082.
- [83] I.S. Fernández, J.D.S. Domingues, T.G. van Kooten, S. Metzger, D.W. Grainger, H. J. Busscher, H.C. van der Mei, Macrophage response to staphylococcal biofilms on crosslinked poly (ethylene) glycol polymer coatings and common biomaterials in vitro, Eur. Cell. Mater. 14 (2011) 73–79.
- [84] M.G. Roy, A. Livraghi-Butrico, A.A. Fletcher, M.M. McElwee, S.E. Evans, R. M. Boerner, S.N. Alexander, L.K. Bellinghausen, A.S. Song, Y.M. Petrova, Muc5b is required for airway defence, Nature 505 (7483) (2014) 412–416.
- [85] L.R. Bonser, D.J. Erle, Airway mucus and asthma: the role of MUC5AC and MUC5B, J. Clin. Med. 6 (12) (2017) 112.
- [86] L.A. Hancock, C.E. Hennessy, G.M. Solomon, E. Dobrinskikh, A. Estrella, N. Hara, D.B. Hill, W.J. Kissner, M.R. Markovetz, D.E.G. Villalon, Muc5b overexpression causes mucociliary dysfunction and enhances lung fibrosis in mice, Nat. Commun. 9 (1) (2018) 1–10.
- [87] D.L. Hughes, A. Hughes, Z. Soonawalla, S. Mukherjee, E. O'Neill, Dynamic physiological culture of ex vivo human tissue: a systematic review, Cancers 13 (12) (2021) 2870.
- [88] S. Böhlen, S. Konzok, J. Labisch, S. Dehmel, D. Schaudien, S. Behrens, F. Schmieder, A. Braun, F. Sonntag, K. Sewald, Using a micro-physiological system to prolong the preservation of ex vivo lung tissue 7 (2) (2021) 207–210.
- [89] T.G. Hayasaki, T.R.M. Santos, A.C.G. Silva, M.C. Valadares, Ex vivo pulmonary assay applied for screening of toxicity potential of chemicals, Food Chem. Toxicol. 161 (2022) 112820.

[90] M. Henjakovic, K. Sewald, S. Switalla, D. Kaiser, M. Müller, T.Z. Veres, C. Martin, S. Uhlig, N. Krug, A. Braun, Ex vivo testing of immune responses in precision-cut lung slices, Toxicol. Appl. Pharmacol. 231 (1) (2008) 68–76.

- [91] A. Wohlsen, C. Martin, E. Vollmer, D. Branscheid, H. Magnussen, W.M. Becker, U. Lepp, S. Uhlig, The early allergic response in small airways of human precisioncut lung slices, Eur. Respir. J. 21 (6) (2003) 1024.
- [92] J. Kirch, M. Guenther, N. Doshi, U.F. Schaefer, M. Schneider, S. Mitragotri, C.-M. Lehr, Mucociliary clearance of micro- and nanoparticles is independent of size, shape and charge—an ex vivo and in silico approach, J. Contr. Release 159 (1) (2012) 128–134.
- [93] E. Harris, M. Easter, J. Ren, S. Krick, J. Barnes, S.M. Rowe, An ex vivo rat trachea model reveals abnormal airway physiology and a gland secretion defect in cystic fibrosis, PLoS One 18 (10) (2023) e0293367.
- [94] A.A. Ammar, M. Gruber, P. Martin, O. Stern, F. Jahshan, O. Ertracht, E. Sela, S. Srouji, E. Zussman, Local delivery of mometasone furoate from an eluting endotracheal tube, J. Contr. Release 272 (2018) 54–61.
- [95] C.-K. Cho, J.-J. Kim, T.-Y. Sung, S.-M. Jung, P.-S. Kang, Endotracheal intubationrelated vocal cord ulcer following general anesthesia, Korean journal of anesthesiology 65 (6 Suppl) (2013) S147.

- [96] K. Chawla, S. Lee, B.P. Lee, J.L. Dalsin, P.B. Messersmith, N.D. Spencer, A novel low-friction surface for biomedical applications: modification of poly (dimethylsiloxane)(PDMS) with polyethylene glycol (PEG)-DOPA-lysine, J. Biomed. Mater. Res. Part A: An Official Journal of The Society for Biomaterials, The Japanese Society for Biomaterials, and The Australian Society for Biomaterials and the Korean Society for Biomaterials 90 (3) (2009) 742–749.
- [97] H.R. Thorarinsdottir, T. Kander, A. Holmberg, S. Petronis, B. Klarin, Biofilm formation on three different endotracheal tubes: a prospective clinical trial, Crit. Care 24 (2020) 1–12.
- [98] O. Diaconu, I. Siriopol, L.I. Poloşanu, I. Grigoraş, Endotracheal tube biofilm and its impact on the pathogenesis of ventilator-associated pneumonia, The Journal of Critical Care Medicine 4 (2) (2018) 50–55.
- [99] A. Radisavljevic, D.B. Stojanovic, S. Perisic, V. Djokic, V. Radojevic, M. Rajilic-Stojanovic, P.S. Uskokovic, Cefazolin-loaded polycaprolactone fibers produced via different electrospinning methods: characterization, drug release and antibacterial effect, Eur. J. Pharmaceut. Sci. 124 (2018) 26–36.